iScience

CellPress
OPEN ACCESS

Article

O-GlcNAcylation regulates OTX2's proteostasis

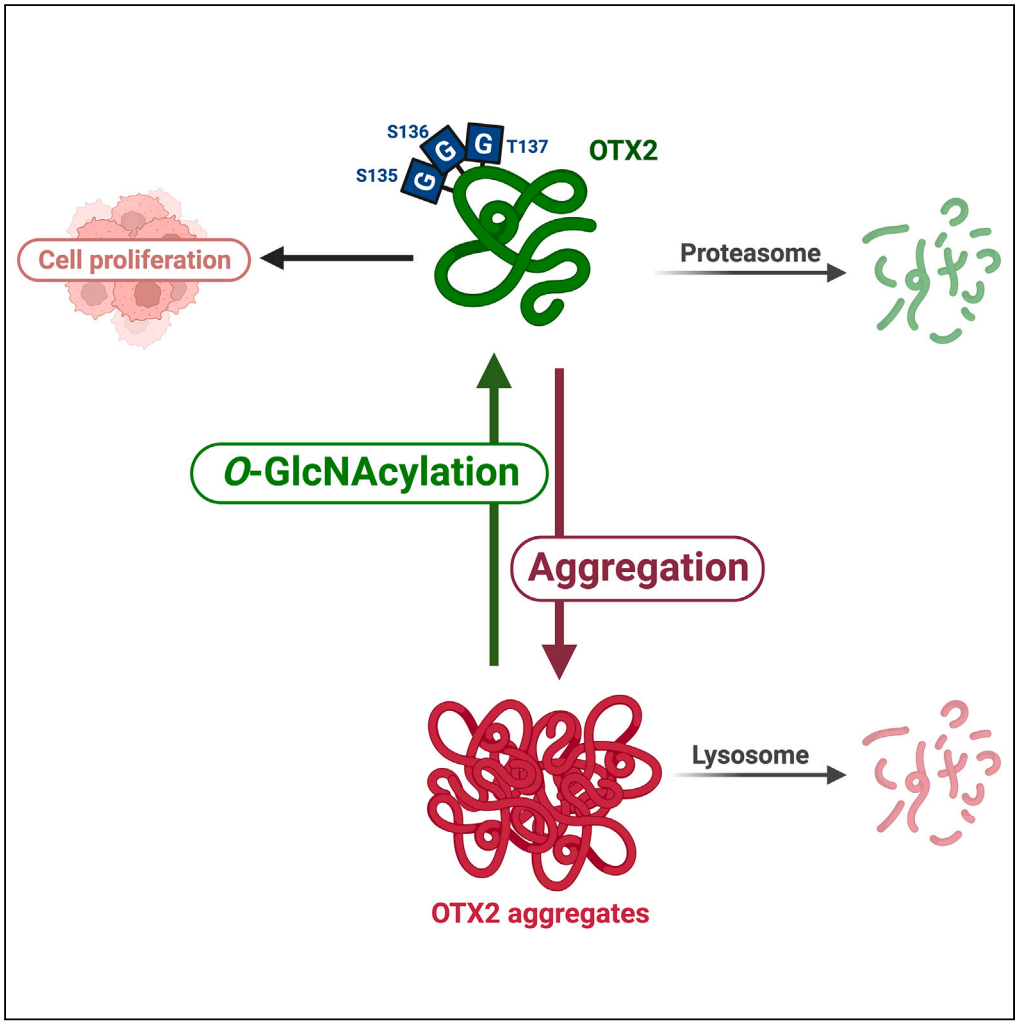

Eugenia Wulff-Fuentes, Jeffrey Boakye, Kaeley Kroenke, ..., Michaela Pereckas, John A. Hanover, Stephanie Olivier-Van Stichelen

solivier@mcw.edu

Highlights

O-GlcNAc stabilizes OTX2 by regulating its autophagy-mediated degradation

O-GlcNAc aids the solubility of OTX2 aggregates

O-GlcNAc-depleted OTX2 loses interaction with the CCT/Chaperonin family of proteins

Wulff-Fuentes et al., iScience *26*, 108184
November 17, 2023
https://doi.org/10.1016/j.isci.2023.108184

iScience

CellPress
OPEN ACCESS

Article

O-GlcNAcylation regulates OTX2's proteostasis

Eugenia Wulff-Fuentes,[1] Jeffrey Boakye,[2] Kaeley Kroenke,[1] Rex R. Berendt,[1] Carla Martinez-Morant,[1] Michaela Pereckas,[1] John A. Hanover,[2] and Stephanie Olivier-Van Stichelen[1,3,4,5,*]

SUMMARY

_O_-GlcNAcylation is a key post-translational modification, playing a vital role in cell signaling during development, especially in the brain. In this study, we investigated the role of _O_-GlcNAcylation in regulating the homeobox protein OTX2, which contributes to various brain disorders, such as combined pituitary hormone deficiency, retinopathy, and medulloblastoma.

Our research demonstrated that, under normal physiological conditions, the proteasome plays a pivotal role in breaking down endogenous OTX2. However, when the levels of OTX2 rise, it forms oligomers and/or aggregates that require macroautophagy for clearance. Intriguingly, we demonstrated that _O_-GlcNAcylation enhances the solubility of OTX2, thereby limiting the formation of these aggregates. Additionally, we unveiled an interaction between OTX2 and the chaperone protein CCT5 at the _O_-GlcNAc sites, suggesting a potential collaborative role in preventing OTX2 aggregation. Finally, our study demonstrated that while OTX2 physiologically promotes cell proliferation, an _O_-GlcNAc-depleted OTX2 is detrimental to cancer cells.

INTRODUCTION

O-GlcNAcylation is a nutrient-dependent post-translational modification (PTM) that has shown potential in designing new treatment options for diseases such as Alzheimer's and cancers.[1,2] Consisting in the addition of a single N-Acetylglucosamine moiety onto serine or threonine residues, *O*-GlcNAcylation modifies more than 8,000 human nuclear, cytoplasmic, and mitochondrial proteins.[3] The *O*-GlcNAc Transferase (OGT) adds the *O*-GlcNAc moiety onto proteins, thereby regulating their localization, stability, interactions, and activity. The *O*-GlcNAcase (OGA) enzyme makes this PTM dynamic by hydrolyzing off the GlcNAc residue. Furthermore, *O*-GlcNAcylation is regulated, in part, by the available pools of its donor substrate, UDP-GlcNAc, which directly reflects extracellular glucose levels.[4] Hence, *O*-GlcNAcylation is a nutrient-sensing PTM. Also, since it modifies identical amino acid residues as phosphorylation, both PTMs often compete or crosstalk to regulate proteins' functions.[5]

Importantly, *O*-GlcNAc is an essential PTM, as evidenced by *Ogt* knockout's (KO) mice embryonic lethality and *Oga* conditional KO's perinatal lethality.[6,7] Efforts to elucidate *O*-GlcNAcylation's role in early development have highlighted cellular processes such as epigenetics, transcription/translation, and cell cycle as critically regulated by *O*-GlcNAcylation.[8–10] In addition, OGT directly modifies transcription factors (TFs) involved in pluripotency, differentiation, and proliferation, making it a critical regulator of development.[11] Additionally, *O*-GlcNAcylation plays a key role in cancer development. All cancer studied to date demonstrates increased *O*-GlcNAcylation levels.[1] While it is unclear whether this is due to the transcriptional upregulation of *O*-GlcNAc enzymes, the switch in glycolytic metabolism (e.g., Warburg effect) in cancers,[4] or both, hyper-*O*-GlcNAcylation has become a cancer hallmark that explains the dysregulation of numerous oncogenes such as β-catenin, c-Myc or Akt.[1]

O-GlcNAcylation levels are elevated in patient samples with medulloblastoma, the most common malignant brain tumor in children, with around 1,500 new cases each year.[12] In a subset of medulloblastoma, OGT stimulates the Sonic hedgehog proliferation signaling pathway by modifying GLI family zinc finger 2 (GLI2).[12] In other subclasses, Orthodenticle homeobox 2 (OTX2) is a relevant oncogene in medulloblastoma described as *O*-GlcNAcylated.[13] However, the function of *O*-GlcNAc on this oncogene has yet to be studied.

OTX2 is a transcription factor that establishes the patterning/delineation of the midbrain and forebrain in early development.[14] Complete ablation of the *Otx2* gene in mice is lethal, and even a heterozygous genotype can lead to loss or malformations of the brain or head.[14] Later in development, OTX2 forms sensory organs and the pituitary and pineal glands. Consequently, *OTX2* mutations are associated with eye diseases such as microphthalmia and anophthalmia, Combined Pituitary Hormone Deficiencies (CPHD), and developmental delays.[15] Additionally, OTX2 is an oncogene in the two most common subclasses of medulloblastomas, where it is overexpressed.[16] *OTX2* knockdown in medulloblastoma cells demonstrated its function in activating cell cycle genes and inhibiting further neuronal differentiation, in line with its

[1]Department of Biochemistry, Medical College of Wisconsin, Milwaukee, WI 53226, USA
[2]Laboratory of Cell and Molecular Biology, National Institute of Diabetes and Digestive and Kidney Diseases, National Institutes of Health, Bethesda, MD 20892-0851, USA
[3]Department of Obstetrics and Gynecology, Medical College of Wisconsin, Milwaukee, WI 53226, USA
[4]X (formerly Twitter): @OVSLab_OGlcNAc
[5]lead contact
*Correspondence: solivier@mcw.edu
https://doi.org/10.1016/j.isci.2023.108184

role as a primed pluripotency transcription factor.[17] Studies on how OTX2 coordinates both activation and repression of target genes highlighted the regulation of OTX2 activity by phosphorylation in its central region (aa 97–178), e.g., Repression/Retention Domain,[18] reinforcing the regulatory role of OTX2 PTMs for its diverse spatial- and time-dependent functions during development. Thus, we interrogated the role of *O*-GlcNAc on OTX2 in a medulloblastoma model.

In this article, we demonstrate that *O*-GlcNAcylation regulates OTX2. We mapped and validated OTX2's *O*-GlcNAc sites and confirmed that it did not compete with its phosphorylation sites. We demonstrated that both the proteasome and macroautophagy regulated OTX2 turnover. While the proteasome remains the canonical degradation pathway, we showed that OTX2 forms soluble oligomers and detergent-resistant aggregates that require macroautophagy for degradation. We established that the elevated cellular concentration of OTX2, following the inhibition of proteasomal degradation or overexpression, promotes its aggregation, while *O*-GlcNAcylation improved its solubility. We determined that OTX2 interacts with the chaperonin CCT5 and other members of the TriC complex, known to participate in protein folding and de-aggregation. Furthermore, this interaction is lost when mutating the *O*-GlcNAc sites in the retention domain, suggesting a protective role of *O*-GlcNAcylation in OTX2 turnover. Finally, while WT OTX2 overexpression enhances cell proliferation, in agreement with its role as an oncogene, an *O*-GlcNAc-depleted OTX2 triggers cytotoxicity.

Our discoveries indicate that the process of aggregating and autophagic degradation of OTX2 may act as a defense mechanism against atypical OTX2 levels, as observed in medulloblastoma. Nonetheless, in the context of cancer marked by excessive *O*-GlcNAcylation, this could stabilize OTX2, thereby contributing to the advancement of cancer.

RESULTS

OTX2 is primarily modified in its central retention domain

We first investigated OTX2 *O*-GlcNAcylation sites. We produced *O*-GlcNAcylated OTX2 by co-overexpressing human FLAG-tagged OTX2 and human OGT cloned in the pETDuet bacterial expression plasmid in BL21 *E. coli* cells (Figure S1A). *O*-GlcNAc-modified OTX2-FLAG was then immunoprecipitated and analyzed by electron-transfer/higher-energy collision dissociation–mass spectrometry (EThcD-MS) (Figures 1A, 1B, S1B, and S1C; Table S1). Three sites were identified in the central domain of OTX2 with high confidence (S135, S136, T137) (Figures 1A, 1B, S1B, and S1C). Additionally, up to 7 more sites were found on additional OTX2 peptides (Figure 1B), as shown by ion masses corresponding to the loss of HexNAc in high collision dissociation (HCD) spectra. However, not enough ions were obtained in the electron transfer dissociation (ETD) spectra to confidently assign a residue to the modification site (Weak EThcD, or HCD only) (Figure 1B; Table S1). The various *O*-GlcNAc sites and peptides mapped were visualized on the AlphaFold predicted 3D structure of OTX2, emphasizing that OGT prefers unstructured protein domains (Figure 1B), as previously suggested.[19]

To observe the abundance of *O*-GlcNAcylation on OTX2, we used various Myc-tagged-OTX2 constructs, including full length (FL), Retention Domain only (RD), which contains the *O*-GlcNAc sites identified previously (S135, S136, T137), and deletion of RD domain (ΔRD) constructs (Figure 1C). Following enrichment for *O*-GlcNAcylated proteins with Wheat Germ Agglutinin (WGA), over 80% of OTX2-FL was pulled down with WGA, confirming that OTX2 is heavily modified (Figures 1C and S1D), which agrees with the previous analysis of OTX2 *O*-GlcNAcylation.[13] Furthermore, OTX2-ΔRD showed markedly decreased binding to WGA (~55%). At the same time, OTX2-RD was heavily pulled down on WGA beads, with a comparable ratio to OTX2-FL (Figure 1C), confirming that most OTX2 *O*-GlcNAcylation sites are contained in the RD domain.

We then confirmed that OTX2 *O*-GlcNAcylation was similar in humans by transfecting an OSF (One-STrEP-FLAG)-tagged OTX2 in HeLa cells (Figure S1E). Cells were additionally treated with Thiamet-G (TG), an OGA inhibitor, to promote *O*-GlcNAcylation. After pulldown with Strep-Tactin beads, EThcD-MS mapping of OTX2-OSF confirmed similar *O*-GlcNAcylated peptides to the previous expression experiment in bacteria (Table S2). Additionally, we verified the presence of *O*-GlcNAcylated OTX2 in a physiological setting. We immunoprecipitated OTX2 from medulloblastoma cells, which express OTX2 due to gene duplication, and observed a signal with an anti-*O*-GlcNAc antibody (Figure S1F).

We verified the *O*-GlcNAc sites using site-directed mutagenesis. The three identified amino acids, S135, S136, and T137, were mutated to alanine, individually or combined. Because OGT is known to move over to adjacent sites when amino acids are mutated,[20] we also mutated S138, individually or combined with the three sites identified. While S135A and S138A mutations did not significantly impact OTX2 *O*-GlcNAcylation levels compared to WT, mutations S136A and T137A demonstrated a 50% decrease in *O*-GlcNAc level (Figures 1D, 1E, and S1G). Furthermore, OTX2 mutants of three or more residues in that sequence also displayed a significant reduction of the *O*-GlcNAc signal compared to WT (Figures 1D and 1E). Thus, we validated that S136 and T137 were the main *O*-GlcNAcylated residues of OTX2. To further examine the role of *O*-GlcNAcylation on OTX2, we elected the triple mutant 3A (S135A/S136A/T137A) for a maximal depletion of OTX2 *O*-GlcNAcylation in the retention domain.

Because OTX2's RD domain is known to be phosphorylated in residues T115, S116, S132, and S158,[18] we were intrigued by the proximity of the phospho-S132 residue next to *O*-GlcNAc sites. Thus, we question whether *O*-GlcNAc might compete with phosphorylation. Therefore, protein extract of HeLa cells transfected with the various domain constructs of OTX2 were resolved in a PhosTag SDS-PAGE, which created mass shifts for OTX2 phosphorylated compared to non-phosphorylated proteins (Figures S1H and S1I). Pre-treatment with Lambda phosphatase removed the upshifted bands, confirming the phospho-gel's specificity (Figure S1J). Analysis of Homeodomain (HD), RD, and the OTX2-transactivation/dimerization domain (OT) OTX2 protein resolved on PhosTag gel confirmed at least three phosphorylated forms for OTX2, on the HD, the RD, and the OT domain (Figure S1H and S1I). This was confirmed by three mass

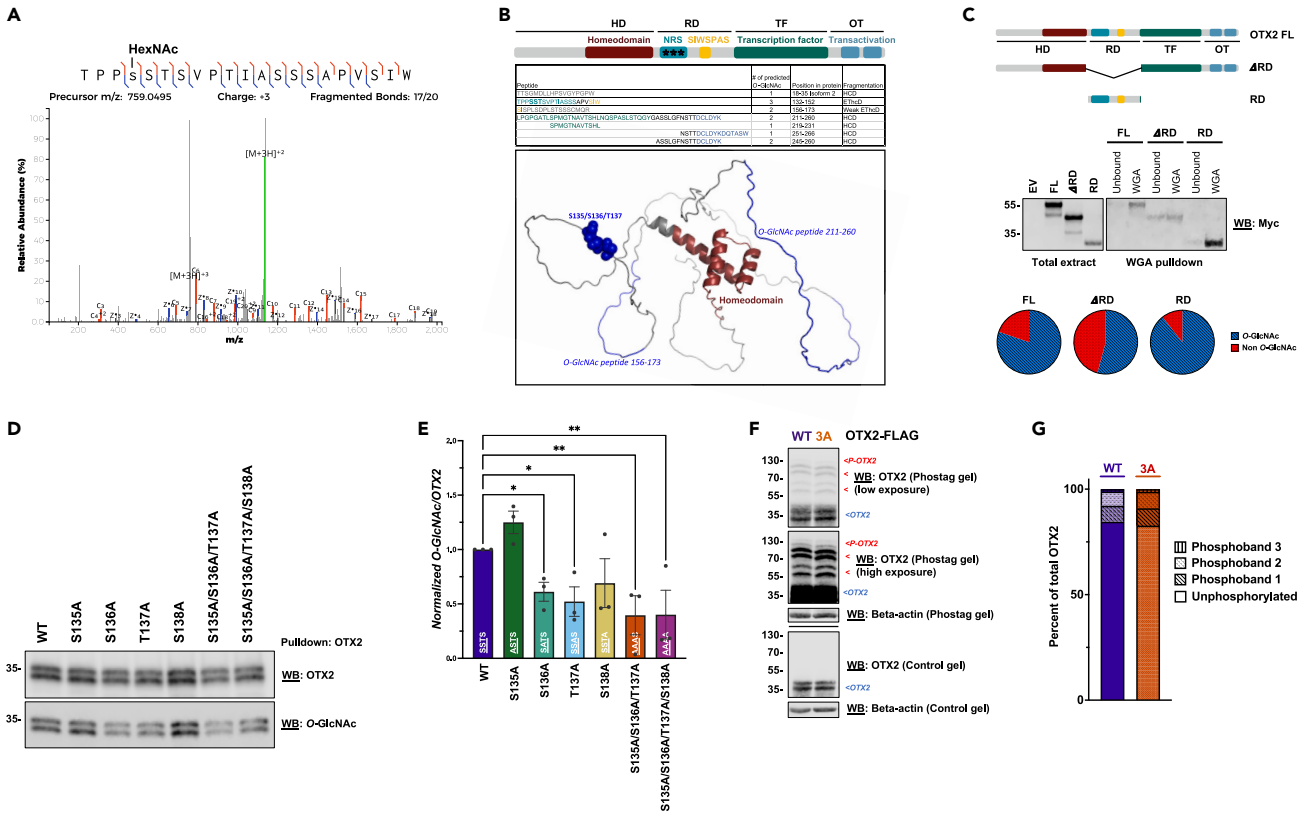

Figure 1. OTX2 is primarily modified in its central retention domain

(A) Electron-transfer/higher-energy collision dissociation–mass spectrometry (EThcD-MS) spectrum of the m/z 759.0495 3+ precursor of an OTX2 peptide modified by HexNAc on serine 135 (lowercase).

(B) Table summary of modified peptides. Stars indicate *O*-GlcNAc sites identified by mass spectrometry. HD, homeodomain; RD, Retention Domain; TF, transcription factor domain; OT, transactivation domain; NRS, nuclear retention sequence; SIWSPAS, corepressor interaction motif. AlphaFold protein structure of OTX2 annotated with the *O*-GlcNAc sites identified (blue spheres), *O*-GlcNAcylated peptides with no specific residue identified (blue ribbon), and the homeodomain (maroon).

(C) WGA pulldown of outlined constructs in HeLa cells. FL, Myc-tagged OTX2 full length; ΔRD, Retention Domain deletion; RD, Retention Domain only. Western blot (WB) bands were quantified as unbound (Non-*O*-GlcNAc) and WGA-bound (*O*-GlcNAc) and normalized to the amount of each construct in the total extract WB.

(D) Immunoblot of pulldowns of OTX2 *O*-GlcNAc site mutants and WT OTX2 transfected into HeLa cells.

(E) Quantification by the optic density of representative blot (D) and biological replicates. One-way ANOVA, $p < 0.05$ (*), $p < 0.01$ (**) (n = 3).

(F) HeLa cells transfected with WT or 3A mutant OTX2. Phosphorylated species were visualized by PhosTag SDS-PAGE.

(G) Optical density quantification (n = 3). Data are represented as mean ± SEM in panels presenting pooled data.

See also Figures S1, S2, Tables S1, and S2.

increments on WT OSF-tagged OTX2 (Figures 1F and 1G). We then treated the cells with TG to promote *O*-GlcNAcylation and observed that it did not significantly perturb the levels of the phosphorylated OTX2 domains (Figures S1H and S1I). Similarly, mutation of the 3 *O*-GlcNAc residues of OTX2 did not impact the phosphorylation status on Phos-tag gels, suggesting that *O*-GlcNAcylation does not compete with phosphorylation on OTX2, nor does it disrupt OTX2's phosphorylation as a whole (Figures 1F and 1G). Therefore, we are confident that throughout the article, the utilization of OTX2 mutants solely represents the impact of OTX2 *O*-GlcNAc depletion rather than phosphorylation.

O-GlcNAcylation does not affect OTX2 subcellular localization

Given that *O*-GlcNAcylation sites are in the nuclear retention domain (Figure 1B), we hypothesized that *O*-GlcNAc regulates OTX2 by controlling its subcellular localization. Thus, we examined the subcellular localization of Myc-tagged OTX2 constructs treated with TG (Figure S2A and S2B). TG treatment did not impact OTX2 localization in nuclear vs. cytoplasmic fractions, even when expressing the highly *O*-GlcNAcylated RD domain of OTX2 (Figure S2A). Further, the localization of GFP-tagged OTX2 was also observed by confocal microscopy in HeLa cells after TG treatment and confirmed the nuclear localization of OTX2 with or without TG treatment (Figure S2C). Furthermore, GFP-tagged *O*-GlcNAc mutants S136A, T137A, and S135A/S136A/T137A (3A) also localized to the nucleus as seen with WT OTX2 in HeLa cells (Figure S2D), supporting that *O*-GlcNAcylation at these residues did not regulate OTX2's nuclear retention.

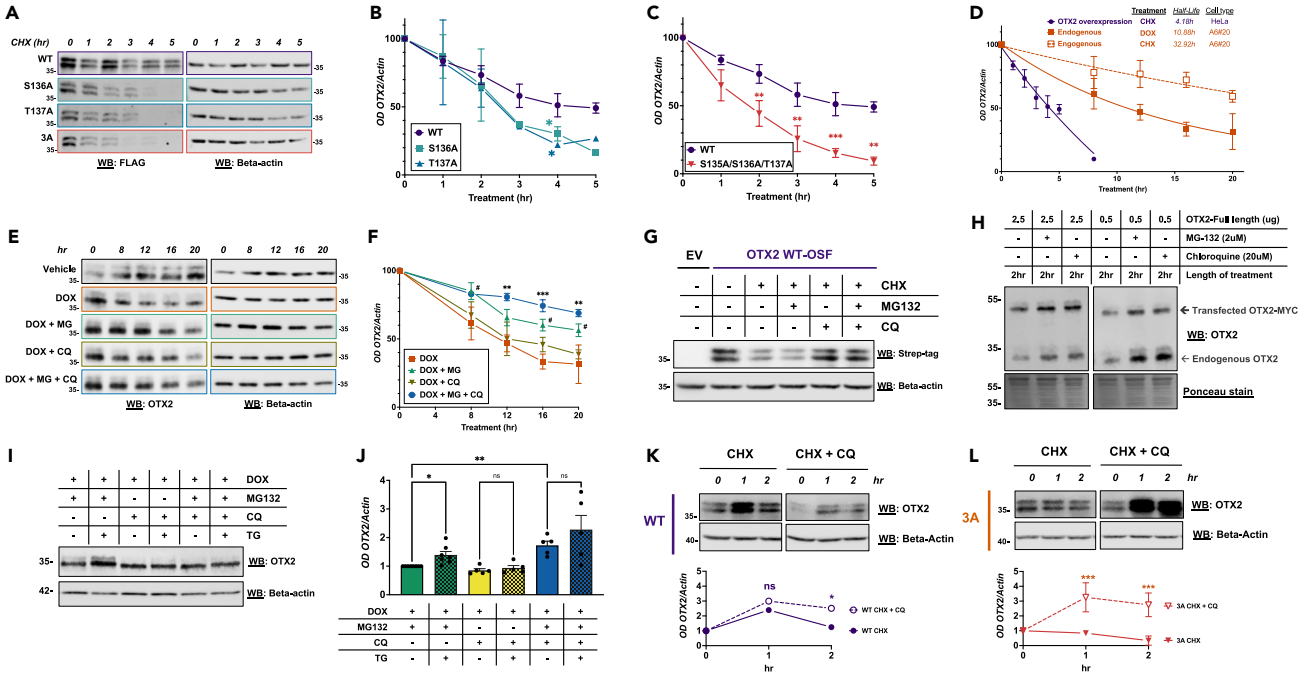

Figure 2. *O*-GlcNAc prevents OTX2 macroautophagy-dependent degradation

(A) HeLa cells transfected with WT OTX2 or *O*-GlcNAc deficient mutants S136A, T137A, or 3A (S135A/S136A/T137A), treated with cycloheximide (CHX) or vehicle for up to 5 h and analyzed by Western Blot (WB).

(B) Optical density (OD) quantification of individual site mutants S136A and T137A. Mutant vs. WT, mixed-effects analysis, $p < 0.05$ (*) (n = 3).

(C) OD quantification of 3A mutant vs. WT, two-way ANOVA, $p < 0.05$ (*), $p < 0.01$ (**) (n = 3).

(D) OTX2 degradation timeline upon Doxycycline (DOX)-triggered *OTX2* KD or CHX treatment for A6#20 human medulloblastoma cells, or CHX treatment for HeLa cells transfected with WT-OTX2. Half-lives were calculated by non-linear regression analysis.

(E) WB of A6#20 cells treated with DOX, MG132, chloroquine (CQ), or vehicle, for up to 20 h.

(F) OD quantification of WB (n = 3). Two-way ANOVA, DOX vs. DOX+MG, $p < 0.05$ (#); DOX vs. DOX+MG+CQ, $p < 0.01$ (**), $p < 0.001$ (***).

(G) A6#20 cells transfected with WT OTX2 were treated with CHX, MG132, CQ, or vehicle overnight.

(H) A6#20 cells transfected with WT OTX2 were treated with MG132, CQ, or vehicles for 2 h.

(I) Western blot of A6#20 medulloblastoma cells treated overnight with MG132, chloroquine (CQ), Thiamet-G (TG), and doxycycline (DOX), individually and in combination.

(J) Quantification of Western blot (I) and biological replicates. One-way ANOVA, $p < 0.05$ (*), $p < 0.01$ (**) (n = 5).

(K and L) HeLa cells transfected with WT (K) or 3A-OTX2 (L) and treated with CHX supplemented with CQ (n = 2), two-way ANOVA, $p < 0.01$ (**), $p < 0.001$ (***).

Data are represented as mean ± SEM in panels presenting pooled data.

See also Figures S3 and S4.

O-GlcNAc depleted OTX2 is less stable

A standard function for *O*-GlcNAcylation is to regulate protein stability.[21] Interestingly, proper OTX2 protein levels are critical in the development and cancer progression.[17] Thus, we then investigated the impact of *O*-GlcNAcylation on OTX2 stability by transfecting the *O*-GlcNAc-depleted mutants in HeLa cells, treated with Cycloheximide (CHX) to inhibit protein synthesis and analyze OTX2's degradation rate (Figures 2A–2C). Both S136A and T137A mutants were less stable than the WT after 3 h of CHX treatment, an effect that was enhanced when observing the degradation of the triple mutant 3A (S135A/S136A/T137A) compared to WT (Figures 2A–2C). Thus, OTX2's main sites of *O*-GlcNAc modification are S136 and T137, and mutations of these sites to alanine, individually or in combination, lead to destabilization and quicker degradation of OTX2. Further supporting that *O*-GlcNAc enhances OTX2 stability, we observed that increased *O*-GlcNAc with TG treatment led to the stabilization of OTX2 even with its neo-synthesis blocked by *OTX2-shRNA* in the endogenous model of medulloblastoma cells (Figure S3A).

OTX2 is degraded by multiple pathways

While OTX2's timely expression and degradation are critical,[17] OTX2 degradation's pathway(s) are unknown. OTX2 is a relatively small nuclear protein with a predicted molecular weight of 32 kDa. Like many oncogenes with short half-lived proteins, we expected OTX2's main degradation route to be the Ubiquitin-Proteasome System (UPS).[22] However, similar transcription factors critical for proliferation and pluripotency, such as OCT4, NANOG, and SOX2, utilize UPS and autophagy mediated-degradation.[23]

To determine OTX2 degradation pathways in a physiological setting, we elected the D425 medulloblastoma cells, which endogenously expressed OTX2, and treated them with CHX to observe the degradation of endogenous OTX2 (Figure 2D). However, OTX2 in D425 cells was surprisingly resistant to CHX treatment compared to HeLa cells (Figure 2D). Therefore, we explored using RNA silencing to efficiently, and more specifically, knockdown OTX2 expression. We elected the A6#20 clone of D425 cells, stably transfected with doxycycline (DOX)-inducible *OTX2* shRNA.[17] Upon DOX treatment, OTX2 half-life was largely diminished (~11 h) compared to CHX treatment (~33 h) (Figure 2D) and agreed with OTX2's previously described half-life.[17] Because of the efficiency and specificity of DOX treatment in medulloblastoma cells, we elected to use this more targeted approach to study the mode of degradation of endogenous OTX2.

Thus, A6#20 cells were treated with DOX and conjointly incubated with either the proteasome inhibitor MG132, the macroautophagy inhibitor chloroquine (CQ), or both for up to 20 h (Figures 2 E and 2F). The efficiency of MG132 treatment was confirmed with the accumulation of ubiquitinated proteins and CQ by increased LC3-II (Figure S3B and S3C). Lipidated LC3 (LC3-II) accumulation correlates with autophagosomes being unable to fuse with lysosomes and complete the macroautophagy flux/degradation (Figure S3B).

While DOX treatment led to a steady degradation of up to 20 h post-treatment, MG132 treatment stabilized OTX2 (Figures 2E and 2F). Furthermore, while CQ alone did not significantly impact OTX2, there was an additional stabilization of OTX2 when conjointly treated with MG132 and CQ treatment compared to MG132 alone (Figures 2E and 2F). A similar result was observed when using CHX instead of DOX, although CHX was less efficient in blocking OTX2 neo-synthesis, as previously noted (Figure S3D–S3H). These observations provided evidence that OTX2 can be degraded not only by proteasomal degradation but also by lysosomal-mediated degradation, and a recent study supports this by discovering the mechanism of OTX2 trafficking to lysosomes.[24]

We then aimed to confirm that both endogenous and exogenous OTX2 behaved similarly in response to the various treatments. Thus, we performed a similar experiment overexpressing WT-OTX2-OSF in A6#20 cells. We first observed that after overnight treatment, overexpressed OTX2 was not stabilized by MG132, suggesting that it was being efficiently degraded (Figure 2G). On the other hand, CQ treatment prevented OTX2 degradation with or without MG132 co-treatment, implying that the lysosome efficiently takes care of overexpressed OTX2 (Figure 2G). Because we observed that exogenous OTX2 was degraded quicker than endogenous (Figure 2D), we wondered if a shorter time course might allow us to monitor both proteasomal and autophagic degradation of overexpressed OTX2. Expectedly, at 2 h, both endogenous and exogenous OTX2 behaved similarly and were stabilized independently by MG132 or CQ (Figure 2H). These observations were not only made in D425 A6#20 medulloblastoma cells (Figures 2G and 2H) but also in MCF7 breast cancer cells (Figue S4A) and HeLa cells (Figure S4B), confirming the universality of OTX2 degradation.

In a recent study, chloroquine inhibited the fusion of OTX2-containing nuclear vesicles with the lysosome independently of macroautophagy.[24] Thus, we used Rapamycin (RP) to stimulate autophagy while blocking the fusion to lysosomes with CQ (Figure S4C). Rapamycin induced further degradation of OTX2 transfected in HeLa cells, and a combination of RP and CQ emphasized the accumulation of OTX2, likely in autophagosomes (Figure S4C). We then co-stained OTX2 and P62/SQSTM1 in HeLa cells and confirmed that OTX2 was localized in autophagosomes in our system (Figure S4D).

Before moving on to the role of *O*-GlcNAcylation in OTX2 proteostasis, we confirmed that the degradation of exogenous OTX2 by the lysosome was not caused by the overexpression system and/or the tagged construct we used. Thus, we demonstrated that OTX2 degradation was similar to Myc-DDK-tagged OTX2 when using a 6xMyc-Tagged OTX2 and untagged OTX2 (Figures S4E and S4F). We also observed that blocking the proteasome even triggers OTX2 degradation in a dose-dependent manner and independently of CHX pre-treatment (Figures S4A and S4E). Another proteasome inhibitor, Bortezomib (BTZ), was tested and confirmed that blocking the proteasome still triggered OTX2 degradation by autophagy (Figure S4B). It was previously reported that blocking the proteasome can induce autophagy,[25] but we did not observe changes in the global autophagy rate upon MG132, measured by LC3B-II levels (Figure S4G). Conversely, we checked that CQ treatment did not impact the proteasome, as seen with total ubiquitinated proteins (Figure S4H). We concluded that the effect we observed was specific to OTX2 rather than dependent on the transfection system or the use of inhibitors.

After this verification, we thus propose that exogenous OTX2 utilizes the same dual regulation of its degradation at a much quicker rate than endogenous OTX2. Therefore, the timing of future experiments was adapted accordingly.

O-GlcNAcylation regulates autophagy-mediated degradation of OTX2

Because we previously observed that an *O*-GlcNAc-depleted OTX2 was less stable (Figures 2A–2C), we next wondered whether *O*-GlcNAcylation prevents OTX2 proteasomal or macroautophagic degradation. In A6#20 D425 cells treated with DOX, we observed that TG treatment further stabilized endogenous OTX2 compared to MG132 treatment alone (Figures 2I and 2J), suggesting that *O*-GlcNAcylation stabilized OTX2 independently of proteasomal inhibition. In contrast, when CQ inhibited macroautophagy, TG had minimal effect on OTX2 protein levels (Figures 2I and 2J). In HeLa cells, TG also did not further stabilize exogenous OTX2 in a background of RP + CQ (Figure S4C). While *O*-GlcNAcylation has been shown to impact the autophagic process directly,[26,27] TG treatment did not directly affect the level of the autophagy marker LC3-II (Figure S3B), suggesting that TG acted on OTX2 in a targeted manner. Finally, further OTX2 stabilization was seen when combining MG132 and CQ, but TG did not further stabilize OTX2 (Figure 2I and 2J), confirming the previous observation. OTX2-3A is less stable in HeLa cells compared to WT OTX2, but it is twice as sensitive to CQ treatment (Figures 2K and 2L). This suggested that mutating the *O*-GlcNAcylation sites on OTX2 led to a less stable mutant that underwent autophagy at a higher rate, emphasizing that *O*-GlcNAcylation protects OTX2 from autophagy-mediated degradation.

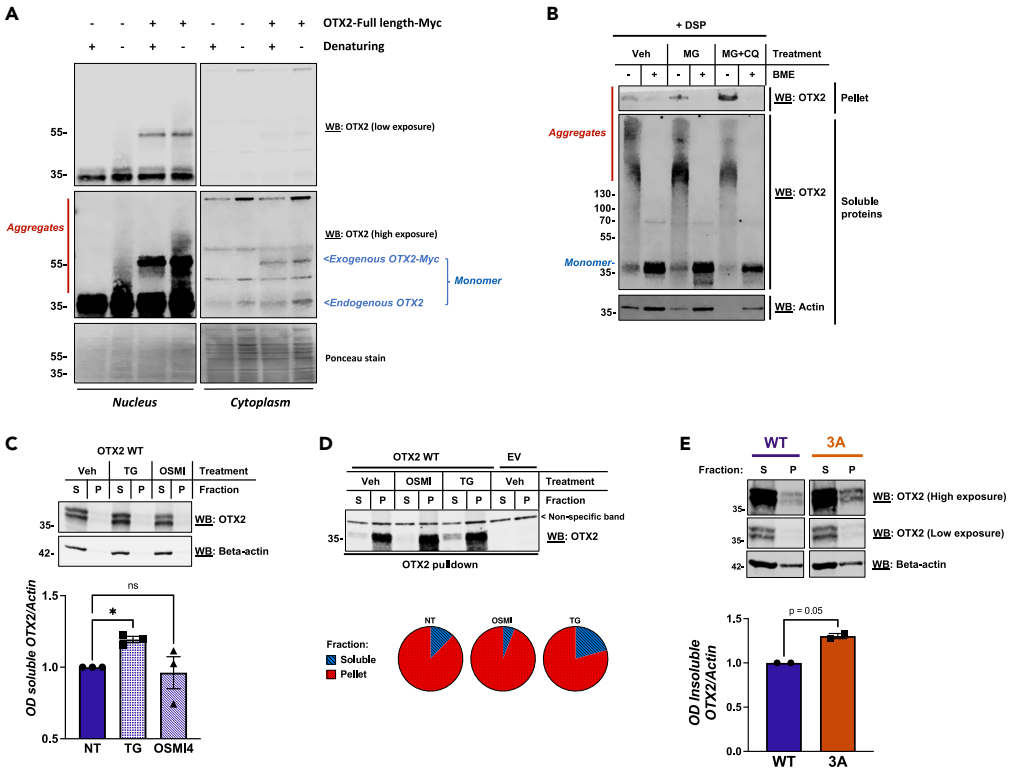

Figure 3. OTX2 aggregation is regulated by *O*-GlcNAcylation

(A) A6#20 cells transfected with WT OTX2 and resolved on SDS-PAGE in denaturing or non-denaturing conditions.

(B) A6#20 cells treated overnight with MG132, chloroquine (CQ), or vehicle and crosslinked with DSP. Samples in either reducing (b-mercaptoethanol, +BME) or non-reducing (-BME) sample buffer were analyzed by WB.

(C and D) HeLa cells were transfected with either WT OTX2 or empty vector (EV-OSF) and treated overnight with the *O*-GlcNAc inhibitors OSMI4, Thiamet-G (TG), or DMSO vehicle. Proteins were crosslinked with DSP at 100 μM (C) or 1 mM (D), lysates separated by soluble and pellet fractions. All samples were run under reducing conditions (+BME), (n = 3), one-way ANOVA, $p < 0.05$ (*). In (D), OTX2 was pulled down with Strep-Tactin beads. Pie charts graph the OD quantification of WB bands in each fraction for each treatment condition.

(E) HeLa cells were transfected with WT or mutant 3A-OTX2. Cells were crosslinked with DSP (100 μM) before harvest, and the soluble and pellet lysates were run under reducing conditions (+BME). Student's *t* test, (n = 2). Data are represented as mean ± SEM in panels presenting pooled data.

See also Figures S5A–S5F.

OTX2 aggregates

We then wondered why a soluble nuclear transcription factor such as OTX2 requires macroautophagy and hypothesized that OTX2 aggregates. We also believe that these aggregates appear when cellular concentrations of OTX2 are elevated, either in response to proteasome inhibition or overexpression. Indeed, overexpression can lead to high protein amounts and, added to proteasome inhibition, create aggregates.[28–30] Furthermore, such as other members of the paired class of homeodomain-containing proteins, OTX2 is known to form homodimers to perform its functions. Still, there have not been investigations of higher-order oligomers containing OTX2.[31]

In D425 medulloblastoma cells, we observed that both endogenous and exogenous OTX2 oligomerizes with higher molecular weight bands appeared in the nucleus in non-denaturing conditions (Figure 3A). In the cytoplasmic fraction, a fraction of OTX2 was also found in the well, suggesting that they were insoluble aggregates of high molecular weight. Because proteins were extracted in detergent-containing lysis buffer, we concluded these aggregates were detergent-resistant.

To stabilize the aggregates, we crosslinked the cells with DSP (dithiobis(succinimidyl propionate))[32] before harvesting the protein lysates (Figures 3B and S5A). However, DSP crosslinking can easily be reversed by adding a reducing agent such as β-mercaptoethanol (BME) (Figure 3B). Moreover, in addition to the soluble supernatant, the insoluble pellet resulting from lysate centrifugation was also loaded on SDS-PAGE to observe insoluble detergent-resistant aggregates. Of note, the entire gel, including the wells, was transferred onto nitrocellulose for western blotting to capture protein aggregate that would not have entered the gel (Figure 3B).

Aggregates were recognized specifically with an OTX2 antibody but not Actin, suggesting that OTX2 formed aggregates with itself or specific interacting partners (Figures 3B and S5B). As predicted, blocking the proteasome with MG132, thus increasing OTX2 cellular concentration, promoted OTX2 aggregation (Figure 3B). Additionally, blocking autophagy with CQ further increased aggregation, suggesting that OTX2 aggregates require macroautophagy for degradation (Figure 3B). This was also reinforced by our previous

experiment in which OTX2 colocalized with p62/SQSTM1, an essential receptor to target protein aggregates to autophagosomes (Figure S4D).

O-GlcNAcylation prevents OTX2 aggregation

We then wondered whether *O*-GlcNAcylation might prevent OTX2 aggregation, as shown for other proteins.[33,34] We used a low (Figure 3C, 100 μM) and high concentration (Figure 3D, 1 mM) of DSP to crosslink OTX2 aggregates. We observed that 100 μM of DSP resulted in mostly soluble OTX2 oligomers/aggregates while 1 mM concentrated OTX2 in the insoluble/pellet fraction (Figure 3C/D, S5A). Nevertheless, in both DSP concentrations, the solubility of OTX2 was increased by treatment with TG and decreased when subjected to OSMI4, an OGT inhibitor that prevented *O*-GlcNAcylation (Figures 3C and 3D; Figure S5C).

In silico analysis of aggregation suggested that 3A-OTX2 aggregated more than WT OTX2, with the introduction of a hot spot with the three amino acid mutation (Figures S5D and S3E). Thus, we observed experimentally a slight increase in OTX2-3A in the insoluble/pellet fraction compared to that seen with WT, supporting that the *O*-GlcNAc-depleted mutant OTX2-3A formed more aggregates than WT (Figure 3E), confirming that *O*-GlcNAcylation assists OTX2 solubility. Finally, we demonstrated that increasing *O*-GlcNAcylation on WT prevented OTX2 aggregation, as evidenced by a lighter signal in the high molecular weight smear with TG. At the same time, it did not impact the aggregated OTX2-3A mutant (Figure S5F), confirming that the *O*-GlcNAcylation of OTX2 S135/S136/T137 facilitates its solubility.

O-GlcNAc-depleted OTX2 loses interaction with the CCT5/Chaperonin family of proteins

We then wondered if *O*-GlcNAc prevented OTX2 aggregation by regulating its interaction with key partners. Thus, the interactome of WT and 3A-OTX2 was analyzed by mass spectrometry after Strep-Tactin pulldown, and changes were measured by label-free quantification normalized to total OTX2 peptides (Figure 4A). Significant gain or loss of interaction was defined as an absolute log2Fold Change >2 and an adjusted p value <0.05. A total of 436 proteins were pulled down as the OTX2 interactome (Table S3). In the individual mutant pulldowns, 39 proteins were significantly dislodged from OTX2 by S136A mutation, while only DNAJC13 bound significantly better to this mutant. On the other hand, 35 interacting partners were lost by mutating T137A on OTX2. We see a consistent loss of protein interactants with all *O*-GlcNAc mutants, including 3A-OTX2, suggesting that both S136 and T137 *O*-GlcNAc modifications perform a similar role (Figure 4A).

To better understand the OTX2 interactome, we built a physical interaction network with the STRING database[35] using all significantly different interactants for each mutant (Figures 4B, S5G and S5H). The common proteins lost by mutating either or all *O*-GlcNAc sites acted in varied biological processes (Figures 4B, S5G, and S5H). Due to our previous demonstration of the impact of *O*-GlcNAc on OTX2 degradation and the convergence of interaction in the STRING network, we identify the Chaperonin Containing TCP1 Subunit 5 (CCT5) protein as a key partner dependent on the 3 *O*-GlcNAcylation sites. Indeed, CCT5 is the central constituent of a node involving protein folding and metabolism amongst the OTX2 interactants (Figure 4B). Interestingly, CCT5 is a member of the T-complex protein Ring Complex (TRiC), also known as the Chaperonin Containing TCP-1 (CCT) complex, which mediates protein folding in the cell. Other members of the TRiC complex also showed decreased interaction with OTX2 mutants (Figure 4C).

Furthermore, CCT5 has also been shown to regulate protein aggregation[36] and would be an excellent candidate to explain the regulation of OTX2 aggregation. Thus, we experimentally confirmed a 40% reduction in CCT5 interaction in 3A-OTX2 pulldown compared to WT OTX2 (Figure 3D). Additionally, we only saw a CCT5/OTX2 interaction in the soluble fraction, suggesting that the TriC complex might help maintain OTX2 solubility rather than de-aggregating OTX2 (Figure 3E).

O-GlcNAcylation in the retention domain does not impact OTX2 transcriptional activity

We then further investigated the functional consequences of OTX2's *O*-GlcNAcylation. Next to OTX2's *O*-GlcNAc sites is an SWISPAS motif (aa 150–159) that determines OTX2's interaction with the corepressor Tle4.[37] To test whether *O*-GlcNAc could impact OTX2's transcriptional activity, we used a SEAP (Secreted alkaline phosphatase) reporter plasmid in which the OTX2-binding *IRBP* promoter was cloned.[38] As expected, treatment with the transcriptional inhibitor DRB (5, 6-dichloro-1-beta-*d*-ribofuranosylbenzimidazole) diminished reporter activity compared to the transfection of OTX2 WT alone, confirming that this was due to the neo-transcription of SEAP following OTX2 promoter binding (Figure 5A). Because *O*-GlcNAcylation impacts transcription, notably through RNA polymerase II,[39] independently of OTX2 (Figure S6A), each OTX2 transfected condition was normalized to its corresponding EV-treated condition. However, OTX2 normalized transcriptional activity was unchanged in WT or 3A-OTX2 transfected cells (Figures 5A and S6A). Furthermore, treatment of cells with OSMI4 did not impact WT OTX2 transcriptional activity. We did observe an increase in transcriptional activity in 3A supplemented with TG that might be linked to other *O*-GlcNAcylation sites on OTX2 (Figure 1B).

OTX2 *O*-GlcNAcylation promotes cell proliferation

Because we know that *O*-GlcNAcylation impacts OTX2 aggregation, we then questioned the impact of OTX2 *O*-GlcNAcylation on cytotoxicity. Thus, we performed an MTT (3-(4,5-dimethylthiazol-2-yl)-2,5-diphenyltetrazolium bromide) cell viability assay using OTX2 WT and 3A mutants combined with *O*-GlcNAc drugs as previously performed. We first observed that the sole transfection of WT OTX2 was sufficient to induce a slight increase in cell viability (Figure 5B), which aligns with the role of OTX2 as an oncogene in medulloblastoma.[40] Because *O*-GlcNAcylation impacts overall cell proliferation,[41] independently of OTX2 (Figure S6B), each OTX2 transfected condition was normalized to its corresponding EV-treated condition. Thus, supplementing the media with OSMI4 further decreased the viability of HeLa cells in an

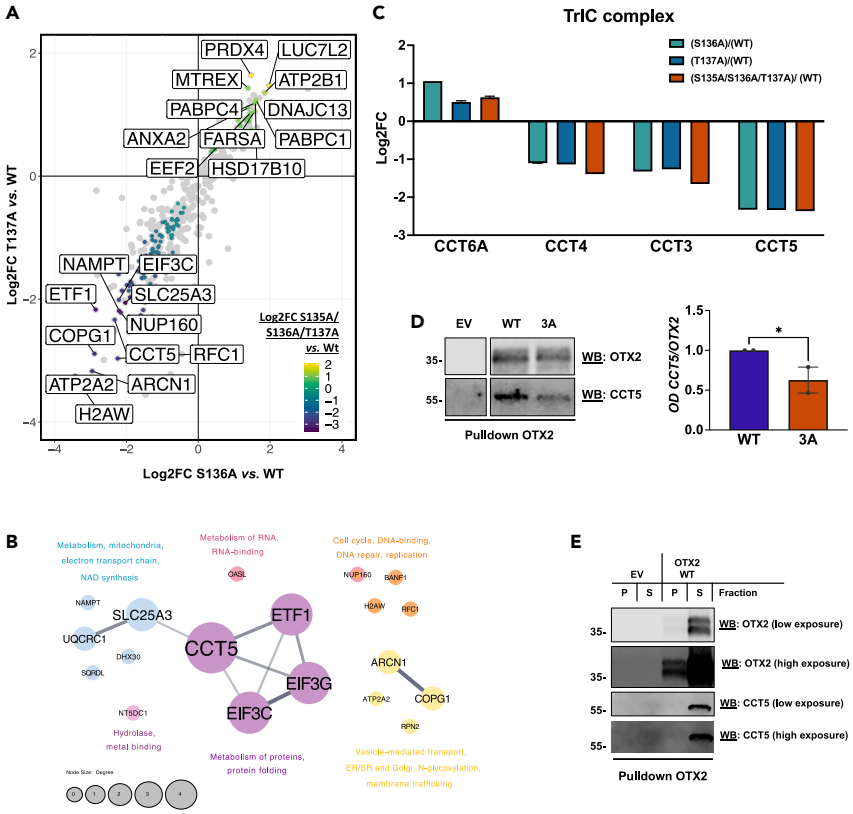

Figure 4. OTX2 *O*-GlcNAc-site mutants lose interactions with the chaperonin CCT5

(A) Volcano plot of proteins commonly lost or gained as OTX2 interactors in WT and mutant constructs (n = 2).

(B) STRING network analysis of the 19 common proteins dislodged from OTX2 when one or all *O*-GlcNAc sites found were mutated to alanine.

(C) Interactome analysis of the TriC complex.

(D) HeLa cells transfected with OTX2 WT or mutant 3A. OTX2 was pulled down and analyzed by Western Blot. Optical density quantification of Western Blot bands. One-way ANOVA, $p < 0.05$ (*) (n = 2).

(E) HeLa cells transfected with OTX2 WT or empty vector EV-OSF, lysates were crosslinked with DSP. OTX2 was pulled down by Strep-Tactin beads from both soluble and pellet fractions and analyzed by Western Blot. Data are represented as mean ± SEM in panels presenting pooled data.

See also Figures S5G, S5H and Table S3.

OTX2-dependent manner (Figures 5C and S6B). Furthermore, transfecting the *O*-GlcNAc-depleted mutant OTX2-3A led to a decrease in cell viability, which was not rescued by the addition of Thiamet-G (Figure 5C). We thus propose that the 3 *O*-GlcNAc sites in the retention domain are essential to prevent cytotoxicity (Figure 5D).

DISCUSSION

Over the years, the key role of *O*-GlcNAcylation in pluripotency is emphasized by the (peri-) lethality of the *O*-GlcNAc enzymes' deletion models in mice, as well as the absence of viable human *O*-GlcNAc enzyme deletions.[7,42] Nevertheless, the discovery of OGT mutations leading to X-linked intellectual disabilities[8] and the meta-analysis of the *O*-GlcNAcome[3] stressed once more the critical role of *O*-GlcNAcylation in early development, particularly in the brain and neighboring structures. Consequently, knocking out *Oga* in the mouse brain leads to severe developmental delays, evident in the brain and pituitary gland.[43] This previous study further emphasized the regulatory differences in the early developmental genes *Sox2*, *Oct4*, and *Otx2*. While the impact of *O*-GlcNAcylation on Sox2 and Oct4 had been previously studied, we pursued the investigation of OTX2/*O*-GlcNAcylation interplay due to OTX2's involvement in early development as well as various pathologies such as retinopathies, CPHD, and medulloblastoma.

OTX2 *O*-GlcNAc modification in the central region

The original discovery of *O*-GlcNAcylation on OTX2 by Ortiz-Meoz et al. highlighted its surprisingly high modification level.[13] Indeed, OTX2 has a high proportion of S/T residues similar to the *O*-GlcNAc semi-consensus sequence,[3] especially in the central domain. We confirmed that OTX2 strongly binds anti-*O*-GlcNAc antibodies in Western blot analysis and binds WGA with high affinity, particularly in the central domain, which seems to contain most *O*-GlcNAc sites. The mapping of *O*-GlcNAcylation sites by mass spectrometry and subsequent mutations of

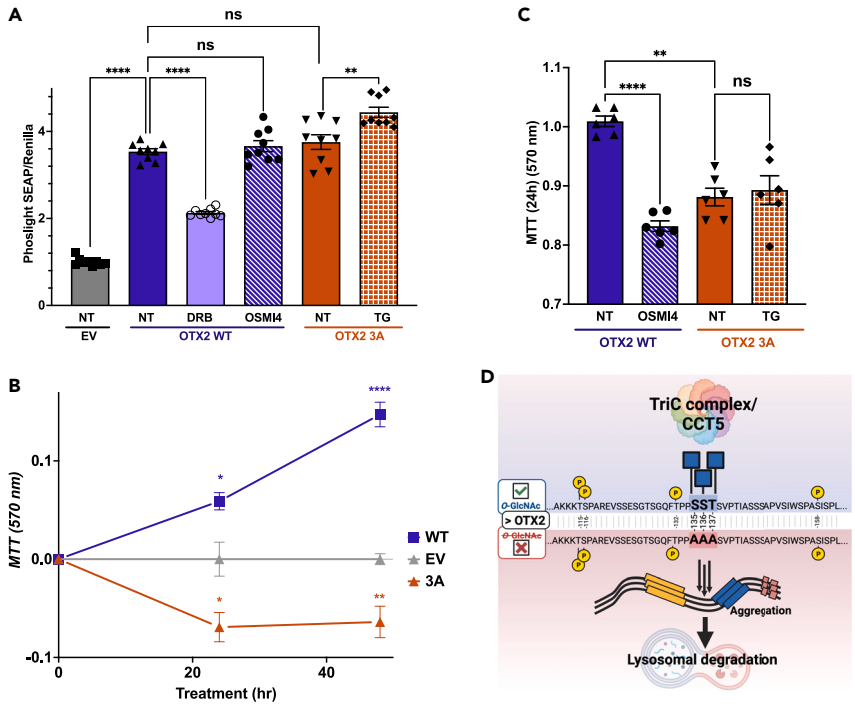

Figure 5. *O*-GlcNAc depleted OTX2 overexpression leads to cytotoxicity

(A) OTX2 transcriptional activity assay of WT- and 3A-OSF constructs in HeLa cells. Activity measured after treatment with TG, OSMI4, or vehicle (NT) (n = 9). Each value was normalized to their corresponding Empty Vector (EV) treated sample. Welch ANOVA, $p < 0.01$ (**), $p < 0.0001$ (****).

(B) MTT assay of HeLa cells transfected with OTX2 WT or 3A mutant for up to 48 h. Each time point value was normalized to the corresponding EV sample (EV: n = 3, WT/3A: n = 6). Multiple unpaired t-tests, $p < 0.05$ (*), $p < 0.01$ (**), $p < 0.0001$ (****).

(C) MTT assay of HeLa cells transfected with OTX2 WT or mutant 3A and treated with OSMI4, TG, or vehicles (NT) for 24 h (n = 6). Each value was normalized to their corresponding EV treatment sample. Welch ANOVA, $p < 0.01$ (**), $p < 0.0001$ (****).

(D) Proposed model of OTX2 turnover regulation by *O*-GlcNAcylation. Created with BioRender.com. Data are represented as mean ± SEM in panels presenting pooled data.

See also Figure S6.

identified residues confirmed that OTX2 is strongly modified at residues S136 and T137. Other regions of OTX2 are also *O*-GlcNAcylated, but while weak EThcD-MS spectra do not allow for the precise identification of *O*-GlcNAc sites, they seem to evade/flank the homeodomain and reside in disordered regions of this protein. This supports the field-known preference of *O*-GlcNAcylation to modify intrinsically disordered proteins/domains.[3] Overall, we estimate that at least eight sites of *O*-GlcNAcylation are present on OTX2.

The heavily modified unstructured central domain of OTX2 contains sequences that (1) retain OTX2 to the nucleus through an unknown mechanism (Nuclear Retention Sequence, NRS)[38]; (2) interact with the corepressor TLE/Groucho using SIWSPAS motif to repress the transcription of target genes[44]; (3) are subjected to phosphorylation (T115, S116, T132 and S158) that change OTX2 activity to either activate or repress the transcription of specific target genes.[18] Despite a nuclear retention domain and phosphorylation residues proximal to OTX2 *O*-GlcNAcylation residues, *O*-GlcNAcylation does not impact OTX2 cellular distribution or phosphorylation level.

OTX2 is degraded by the proteasome and, when aggregated, by autophagy

Literature supports our findings in medulloblastoma cells that OTX2 is principally degraded by the Ubiquitin Proteasome System (UPS), as suggested briefly by a previous study in mESCs.[45] However, the ubiquitin ligase and regulation of ubiquitination of OTX2 are unknown. Previous literature and our findings provide a few candidates worth pursuing. First, a study by Vriend and Rastegar analyzed publicly available gene expression databases to identify E3 ligases or adaptors as genetic markers of medulloblastoma subtypes.[46] They identified E3 ligase DCUN1D2 and adaptor PPP2R2C as negatively correlated with the expression of OTX2.[46] Other candidates include the E3 ligase-related proteins CUL4A and UBR4 from our OTX2 interactome and the E3 ligase Trip12 from adult neural mouse retina.[47]

While the proteasome degrades OTX2, we also demonstrate that additional stabilization is obtained by blocking the macroautophagy pathway, suggesting that OTX2 uses both degradation modes. Instances of cooperation between these systems to regulate the same target proteins is an established yet little-known phenomenon.[48] Interestingly, similar pluripotency proteins SOX2, OCT4, and NANOG are degraded with different kinetics by the UPS and macroautophagy according to nutrient levels in human ESCs.[23]

In our hands, endogenous OTX2 only utilizes macroautophagy as a secondary degradation when the proteasome is inhibited, which leads to an increased cellular concentration of OTX2. This effect was accentuated when exogenously expressing OTX2 due to the excessive amounts of protein produced by the CMV-driven plasmid promoter. Indeed, the high concentrations of proteins due to overexpression can overload specific biological pathways, disrupt protein regulation, or create aggregates.[28] In addition, protein overexpression can also exhaust cell resources to make and transport proteins.[49]

We have demonstrated that OTX2 forms oligomers and/or aggregates resistant to proteasome degradation and require macroautophagy for clearance. A study on OTX2 transport via nuclear budding to the lysosome has recently supported this concept.[24] This study also observed OTX2 stabilization upon overexpression and treatment with lysosomal degradation inhibitors. However, co-localization of OTX2 with autophagosomes was not observed. Our unique experimental setup included using Rapamycin to stimulate autophagy and CQ to block lysosomal fusion, enabling the visualization of OTX2 in autophagosomes. Therefore, in addition to the previously described direct route from the nucleus to the lysosome, our study provides evidence that OTX2 can also utilize macroautophagy for transport to the lysosome for degradation when it is in an aggregated state.Additionally, the OTX2 sequence does contain a poly-glutamine stretch (PolyQ) (102–109aa) at the junction of the homeodomain and the central repression/retention domain, providing a possible avenue for oligomerization/aggregation.

Besides the pluripotency factors mentioned above, several oncogenic transcription factors are degraded by macroautophagy, such as p53, β-catenin, p65, and HIF2a.[50–53] However, there are variations in whether these degradation substrates are ubiquitinated or not, in their native form or aggregated. Nevertheless, it is the norm for soluble single proteins to be degraded by the UPS. In contrast, macroautophagy selectively degrades protein aggregates through receptor recognition and the rest of the process, termed aggrephagy in this context.[54] In this context, we provide evidence that OTX2 does colocalize with p62/SQSTM1 (sequestosome 1), a receptor that shuttles aggregating proteins to autophagosomes to be degraded by the lysosome. In summary, OTX2 aggregates, partly due to its central *O*-GlcNAcylated domain, driving the requirement for macroautophagy.

O-GlcNAcylation participates in regulating OTX2 turnover

O-GlcNAc regulates bulk protein turnover by acting on the main degradation machinery. The proteasome is inhibited by increased *O*-GlcNAc levels, and subunits of the proteasome itself are modified by *O*-GlcNAcylation.[55] On the other hand, low *O*-GlcNAc levels stimulate autophagic flux in mammalian cells,[26] while decreasing *O*-GlcNAc levels in mouse astrocytes increased autophagy.[27] Considering these broad effects of *O*-GlcNAc on protein degradation pathways, it is challenging to assess how *O*-GlcNAc explicitly impacts the degradation of OTX2. By using a targeted approach to mutate *O*-GlcNAcylated sites on OTX2, we demonstrated that losing *O*-GlcNAc sites leads to the destabilization of OTX2 and rapid degradation, suggesting that *O*-GlcNAc directly protects OTX2 from degradation. There are examples of this protection that have been elucidated. The tumor suppressor p53 is stabilized when *O*-GlcNAcylated by reducing its phosphorylation-dependent ubiquitination.[56] The ubiquitous Sp1 transcription factor is deglycosylated under nutrient starvation and is promptly degraded by the proteasome,[57] and the oncogene beta-catenin degradation sequence is inhibited by *O*-GlcNAcylation.[58] Similarly, based on our findings, *O*-GlcNAcylation protects OTX2 from aggregation and subsequent macroautophagy. A similar effect of protein *O*-GlcNAcylation is deeply studied, as it can decrease aggregation and cytotoxicity generated by Tau-containing neurofibrillary tangles and fibrillar α-Synuclein.[34]

CCT5 and the TRiC complex facilitate the solubilization of OTX2 through the retention domain

By mutating *O*-GlcNAcylation sites, critical interactants of OTX2 are displaced, including the chaperonin complex member CCT5 and other members of the chaperonin-containing T-complex (TRiC). It consists of 8 subunit proteins, and although it was first considered to only mediate the folding of the cytoskeleton proteins actin and tubulin, it is now known to assist the folding of various cytosolic proteins, such as the transcription factor p53.[59] Importantly, CCT can lower aggregation and toxicity of Huntingtin (HTT) in Huntington's Disease.[36] Because this complex is required for autophagosome degradation, the clearance of accumulated HTT proteins promoted by CCT is through autophagy.[60] Thus, we imagine that OTX2 will be similarly managed, interacting with CCT mainly through the interaction of CCT5 with the central domain of OTX2 to prevent OTX2 aggregation.

OTX2 *O*-GlcNAcylation promotes cell proliferation

OTX2 overexpression is a key factor in the development of medulloblastoma, where the duplication of its gene renders this protein oncogenic.[16] As previously demonstrated, all cancers present with increased *O*-GlcNAcylation levels, including medulloblastomas.[12] We showed that increased *O*-GlcNAcylation impacts OTX2 proteostasis, leading to its stabilization, which promotes cell proliferation. In normal and healthy cells, we suggest that the aggregation and degradation of OTX2 by macroautophagy is a protective measure to prevent abnormal cell proliferation. However, we propose that, in medulloblastoma cells the metabolic switch happening in cancer development known as the Warburg effect would naturally promote and maintain high *O*-GlcNAcylation levels, thus enhancing the solubility of OTX2 and promoting cell viability. This phenomenon can explain how, without further genomic alteration, cells might increase cell proliferation based on metabolic cues. However, when *O*-GlcNAc is absent or cannot be added due to point mutations, OTX2 becomes cytotoxic.

The OTX2 sequence between humans and mice differs in one amino acid residue (T115->S115). This high conservation emphasizes the essential nature of this protein throughout evolution/across organisms.[61] Complete knockout of this gene is embryonic lethal, and heterozygous mice suffer craniofacial malformations that vary in severity.[14] Thus, Otx2 is essential for developing the brain, pituitary gland, and eyes, and consequently, human mutations often lead to microphthalmia, anophthalmia, combined pituitary hormone deficiency, learning

difficulties, and retinal dystrophies.[62] Interestingly, there appears to be a threshold of OTX2 expression or activity that tips a specific transcriptional landscape toward diseases.[63,64] These previous observations and our findings can explain previously unknown disease mechanisms. For example, most patient mutations concentrate in the middle region of OTX2, proximal to *O*-GlcNAcylation sites, which would normally prevent OTX2 aggregation (Figure S6C).

Additionally, several mutant variants mutate Proline P133 and P134 residues,[38] which are advantageous for the *O*-GlcNAc modification of S/T (P at −2 and −3) based on the semi-consensus sequence[3] (Figures S6D and S6E). In summary, we suggest that in OTX2-related diseases, gene duplication and mutations in the central domain preventing *O*-GlcNAcylation or interaction with the CCT complex increase the OTX2 aggregation and cytotoxicity. Further research is required to investigate this mechanism *in vivo* and explore new avenues in diagnosing and treating OTX2-driven diseases.

Limitations of the study

Some limitations of the study are as follows: (1) we are yet to explore the precise mechanisms through which *O*-GlcNAcylation affords protection against OTX2 aggregation, as well as the nature and dimensions of the aggregates formed by OTX2; (2) In this study, we validated that CCT5 interacts with OTX2, and there is a decrease in that interaction with the 3A mutant, however, how *O*-GlcNAc mediates this interaction and how the CCT complex cooperates to maintain OTX2 levels is yet to be determined; (3) While we observed cytotoxicity following the transfection of *O*-GlcNAc-depleted OTX2, we did not investigate whether this a direct consequence of OTX2 aggregation; (4) The consequences of clinically relevant mutation of OTX2 on its *O*-GlcNAcylation still need to be explored.

STAR★METHODS

Detailed methods are provided in the online version of this paper and include the following:

- KEY RESOURCES TABLE
- RESOURCE AVAILABILITY
  - Lead contact
  - Materials availability
  - Data and code availability
- EXPERIMENTAL MODEL
  - Cell culture
  - Recombinant protein expression in E. coli
- METHOD DETAILS
  - Drugs and inhibitors
  - Plasmids and transient transfections
  - RNA extraction, cDNA synthesis, and quantitative PCR
  - Primers
  - Cell lysis
  - Nuclear and cytosol fractionation
  - Immunoprecipitation (IP) and pulldowns
  - SDS-PAGE and western blotting
  - PhosTag gels
  - SEAP gene reporter assay
  - Protein aggregation assay
  - Antibodies
  - Confocal microscopy
  - MTT cell proliferation assay
  - Mass spectrometry
  - In silico analysis
- QUANTIFICATION AND STATISTICAL ANALYSIS

SUPPLEMENTAL INFORMATION

Supplemental information can be found online at https://doi.org/10.1016/j.isci.2023.108184.

ACKNOWLEDGMENTS

We want to thank John A. Hanover, Ph.D. (NIH) for his constant mentoring, advice, and editing; Rogier Versteeg, PhD (Academic Medical Center, Amsterdam), and Marcel Kool, Ph.D. (Heidelberg University Hospital, Germany) for the A6#20 D425 medulloblastoma cell line; Thomas Lamonerie, Ph.D. (Université Côte d'Azur, Nice, France) for the OTX2-GFP and IRBP-SEAP plasmids; Dawn Wenzel, Ph.D. (MCW) for the OSF plasmid and purification guidance; Elizabeth Sweeney, Ph.D. (MCW) for advice on the DSP crosslink experiments; and the

members of the Olivier-Van Stichelen lab for collegial support and helpful discussions. This work was supported by the National Institute of Child Health and Human Development (R00HD087430, R01HD104808).

AUTHOR CONTRIBUTIONS

Conceptualization, EWF, JAH, and SOVS; methodology, EWF, JB, KK, RRB, CMM, MP, and SOVS; formal analysis, EWF, MP, and SOVS; writing—original draft preparation, EWF; writing—review and editing, EWF, MP, JB, RRB, KK, CMM, JAH, and SOVS; supervision, JAH and SOVS; funding acquisition, JAH and SOVS. All authors have read and agreed to the published version of the article.

DECLARATION OF INTERESTS

The authors declare no competing interests.

INCLUSION AND DIVERSITY

We support inclusive, diverse, and equitable conduct of research. One or more of the authors of this paper self-identifies as an underrepresented ethnic minority in their field of research or within their geographical location. One or more of the authors of this paper self-identifies as a gender minority in their field of research. One or more of the authors of this paper self-identifies as a member of the LGBTQIA+ community.

Received: May 24, 2023
Revised: August 28, 2023
Accepted: October 9, 2023
Published: October 12, 2023

REFERENCES

1. Lee, J.B., Pyo, K.-H., and Kim, H.R. (2021). Role and Function of O-GlcNAcylation in Cancer. Cancers *13*, 5365. https://doi.org/10.3390/cancers13215365.
2. Park, J., Lai, M.K.P., Arumugam, T.V., and Jo, D.-G. (2020). O-GlcNAcylation as a Therapeutic Target for Alzheimer's Disease. NeuroMolecular Med. *22*, 171–193. https://doi.org/10.1007/s12017-019-08584-0.
3. Wulff-Fuentes, E., Berendt, R.R., Massman, L., Danner, L., Malard, F., Vora, J., Kahsay, R., and Olivier-Van Stichelen, S. (2021). The human O-GlcNAcome database and meta-analysis. Sci. Data *8*, 25. https://doi.org/10.1038/s41597-021-00810-4.
4. Akella, N.M., Ciraku, L., and Reginato, M.J. (2019). Fueling the fire: emerging role of the hexosamine biosynthetic pathway in cancer. BMC Biol. *17*, 52. https://doi.org/10.1186/s12915-019-0671-3.
5. Hart, G.W., Slawson, C., Ramirez-Correa, G., and Lagerlof, O. (2011). Cross Talk Between O-GlcNAcylation and Phosphorylation: Roles in Signaling, Transcription, and Chronic Disease. Annu. Rev. Biochem. *80*, 825–858. https://doi.org/10.1146/annurev-biochem-060608-102511.
6. O'Donnell, N., Zachara, N.E., Hart, G.W., and Marth, J.D. (2004). *Ogt* -Dependent X-Chromosome-Linked Protein Glycosylation Is a Requisite Modification in Somatic Cell Function and Embryo Viability. Mol. Cell Biol. *24*, 1680–1690. https://doi.org/10.1128/MCB.24.4.1680-1690.2004.
7. Keembiyehetty, C., Love, D.C., Harwood, K.R., Gavrilova, O., Comly, M.E., and Hanover, J.A. (2015). Conditional Knock-out Reveals a Requirement for O-Linked N-Acetylglucosaminase (O-GlcNAcase) in Metabolic Homeostasis. J. Biol. Chem. *290*, 7097–7113. https://doi.org/10.1074/jbc.M114.617779.
8. Konzman, D., Abramowitz, L.K., Steenackers, A., Mukherjee, M.M., Na, H.-J., and Hanover, J.A. (2020). O-GlcNAc: Regulator of Signaling and Epigenetics Linked to X-linked Intellectual Disability. Front. Genet. *11*, 605263. https://doi.org/10.3389/fgene.2020.605263.
9. Li, X., Zhu, Q., Shi, X., Cheng, Y., Li, X., Xu, H., Duan, X., Hsieh-Wilson, L.C., Chu, J., Pelletier, J., et al. (2019). O-GlcNAcylation of core components of the translation initiation machinery regulates protein synthesis. Proc. Natl. Acad. Sci. USA *116*, 7857–7866. https://doi.org/10.1073/pnas.1813026116.
10. Liu, C., and Li, J. (2018). O-GlcNAc: A Sweetheart of the Cell Cycle and DNA Damage Response. Front. Endocrinol. *9*, 415. https://doi.org/10.3389/fendo.2018.00415.
11. Özcan, S., Andrali, S.S., and Cantrell, J.E.L. (2010). Modulation of transcription factor function by O-GlcNAc modification. Biochim. Biophys. Acta *1799*, 353–364. https://doi.org/10.1016/j.bbagrm.2010.02.005.
12. Chen, L., Li, Y., Song, Z., Xue, S., Liu, F., Chang, X., Wu, Y., Duan, X., and Wu, H. (2022). O-GlcNAcylation promotes cerebellum development and medulloblastoma oncogenesis via SHH signaling. Proc. Natl. Acad. Sci. USA *119*, e2202821119. https://doi.org/10.1073/pnas.2202821119.
13. Ortiz-Meoz, R.F., Merbl, Y., Kirschner, M.W., and Walker, S. (2014). Microarray Discovery of New OGT Substrates: The Medulloblastoma Oncogene OTX2 Is O-GlcNAcylated. J. Am. Chem. Soc. *136*, 4845–4848. https://doi.org/10.1021/ja500451w.
14. Acampora, D., Mazan, S., Lallemand, Y., Avantaggiato, V., Maury, M., Simeone, A., and Brûlet, P. (1995). Forebrain and midbrain regions are deleted in Otx2−/− mutants due to a defective anterior neuroectoderm specification during gastrulation. Development *121*, 3279–3290. https://doi.org/10.1242/dev.121.10.3279.
15. Beby, F., and Lamonerie, T. (2013). The homeobox gene Otx2 in development and disease. Exp. Eye Res. *111*, 9–16. https://doi.org/10.1016/j.exer.2013.03.007.
16. Figueira Muoio, V.M., Uno, M., Oba-Shinjo, S., da Silva, R., Araújo Pereira, B.J., Clara, C., Matushita, H., and Marie, S.N.K. (2019). OTX1 and OTX2 Genes in Medulloblastoma. World Neurosurg. *127*, e58–e64. https://doi.org/10.1016/j.wneu.2019.02.013.
17. Bunt, J., Hasselt, N.E., Zwijnenburg, D.A., Hamdi, M., Koster, J., Versteeg, R., and Kool, M. (2012). OTX2 directly activates cell cycle genes and inhibits differentiation in medulloblastoma cells. Int. J. Cancer *131*, E21–E32. https://doi.org/10.1002/ijc.26474.
18. Satou, Y., Minami, K., Hosono, E., Okada, H., Yasuoka, Y., Shibano, T., Tanaka, T., and Taira, M. (2018). Phosphorylation states change Otx2 activity for cell proliferation and patterning in the Xenopus embryo. Dev. Camb. Engl. *145*, dev159640. https://doi.org/10.1242/dev.159640.
19. Britto-Borges, T., and Barton, G.J. (2017). A study of the structural properties of sites modified by the O-linked 6-N-acetylglucosamine transferase. PLoS One *12*, e0184405. https://doi.org/10.1371/journal.pone.0184405.
20. Pedowitz, N.J., Batt, A.R., Darabedian, N., and Pratt, M.R. (2021). MYPT1 O-GlcNAc modification regulates sphingosine-1-phosphate mediated contraction. Nat. Chem. Biol. *17*, 169–177. https://doi.org/10.1038/s41589-020-0640-8.
21. Akan, I., Olivier-Van Stichelen, S., Bond, M.R., and Hanover, J.A. (2018). Nutrient-driven O-GlcNAc in proteostasis and neurodegeneration. J. Neurochem. *144*, 7–34. https://doi.org/10.1111/jnc.14242.
22. Ciechanover, A., DiGiuseppe, J.A., Bercovich, B., Orian, A., Richter, J.D., Schwartz, A.L., and Brodeur, G.M. (1991). Degradation of nuclear oncoproteins by the ubiquitin system in vitro. Proc. Natl. Acad. Sci. USA *88*, 139–143. https://doi.org/10.1073/pnas.88.1.139.
23. Cho, Y.-H., Han, K.-M., Kim, D., Lee, J., Lee, S.-H., Choi, K.-W., Kim, J., and Han, Y.-M. (2014). Autophagy regulates homeostasis of

pluripotency-associated proteins in hESCs. Stem Cell. *32*, 424–435. https://doi.org/10.1002/stem.1589.

24. Park, J.W., Lee, E.J., Moon, E., Kim, H.-L., Kim, I.-B., Hodzic, D., Kim, N., Kweon, H.-S., and Kim, J.W. (2023). Orthodenticle homeobox 2 is transported to lysosomes by nuclear budding vesicles. Nat. Commun. *14*, 1111. https://doi.org/10.1038/s41467-023-36697-5.
25. Bao, W., Gu, Y., Ta, L., Wang, K., and Xu, Z. (2016). Induction of autophagy by the MG-132 proteasome inhibitor is associated with endoplasmic reticulum stress in MCF-7 cells. Mol. Med. Rep. *13*, 796–804. https://doi.org/10.3892/mmr.2015.4599.
26. Guo, B., Liang, Q., Li, L., Hu, Z., Wu, F., Zhang, P., Ma, Y., Zhao, B., Kovács, A.L., Zhang, Z., et al. (2014). O-GlcNAc-modification of SNAP-29 regulates autophagosome maturation. Nat. Cell Biol. *16*, 1215–1226. https://doi.org/10.1038/ncb3066.
27. Rahman, M.A., Hwang, H., Cho, Y., and Rhim, H. (2019). Modulation of O-GlcNAcylation Regulates Autophagy in Cortical Astrocytes. Oxid. Med. Cell. Longev. *2019*, 6279313. https://doi.org/10.1155/2019/6279313.
28. Vavouri, T., Semple, J.I., Garcia-Verdugo, R., and Lehner, B. (2009). Intrinsic protein disorder and interaction promiscuity are widely associated with dosage sensitivity. Cell *138*, 198–208. https://doi.org/10.1016/j.cell.2009.04.029.
29. Tang, Y.-C., and Amon, A. (2013). Gene copy-number alterations: a cost-benefit analysis. Cell *152*, 394–405. https://doi.org/10.1016/j.cell.2012.11.043.
30. Makanae, K., Kintaka, R., Makino, T., Kitano, H., and Moriya, H. (2013). Identification of dosage-sensitive genes in Saccharomyces cerevisiae using the genetic tug-of-war method. Genome Res. *23*, 300–311. https://doi.org/10.1101/gr.146662.112.
31. Briata, P., Ilengo, C., Bobola, N., and Corte, G. (1999). Binding properties of the human homeodomain protein OTX2 to a DNA target sequence. FEBS Lett. *445*, 160–164. https://doi.org/10.1016/S0014-5793(99)00113-1.
32. Balasubramaniam, M., Ayyadevara, S., Ganne, A., Kakraba, S., Penthala, N.R., Du, X., Crooks, P.A., Griffin, S.T., and Shmookler Reis, R.J. (2019). Aggregate Interactome Based on Protein Cross-linking Interfaces Predicts Drug Targets to Limit Aggregation in Neurodegenerative Diseases. iScience *20*, 248–264. https://doi.org/10.1016/j.isci.2019.09.026.
33. Gambetta, M.C., and Müller, J. (2014). O-GlcNAcylation prevents aggregation of the Polycomb group repressor polyhomeotic. Dev. Cell *31*, 629–639. https://doi.org/10.1016/j.devcel.2014.10.020.
34. Ryan, P., Xu, M., Davey, A.K., Danon, J.J., Mellick, G.D., Kassiou, M., and Rudrawar, S. (2019). O-GlcNAc Modification Protects against Protein Misfolding and Aggregation in Neurodegenerative Disease. ACS Chem. Neurosci. *10*, 2209–2221. https://doi.org/10.1021/acschemneuro.9b00143.
35. Szklarczyk, D., Franceschini, A., Wyder, S., Forslund, K., Heller, D., Huerta-Cepas, J., Simonovic, M., Roth, A., Santos, A., Tsafou, K.P., et al. (2015). STRING v10: protein–protein interaction networks, integrated over the tree of life. Nucleic Acids Res. *43*, D447–D452. https://doi.org/10.1093/nar/gku1003.
36. Tam, S., Spiess, C., Auyeung, W., Joachimiak, L., Chen, B., Poirier, M.A., and Frydman, J. (2009). The chaperonin TRiC blocks a huntingtin sequence element that promotes the conformational switch to aggregation. Nat. Struct. Mol. Biol. *16*, 1279–1285. https://doi.org/10.1038/nsmb.1700.
37. Agoston, Z., and Schulte, D. (2009). Meis2 competes with the Groucho co-repressor Tle4 for binding to Otx2 and specifies tectal fate without induction of a secondary midbrain-hindbrain boundary organizer. Development *136*, 3311–3322. https://doi.org/10.1242/dev.037770.
38. Chatelain, G., Fossat, N., Brun, G., and Lamonerie, T. (2006). Molecular dissection reveals decreased activity and not dominant negative effect in human OTX2 mutants. J. Mol. Med. *84*, 604–615. https://doi.org/10.1007/s00109-006-0048-2.
39. Parker, M.P., Peterson, K.R., and Slawson, C. (2021). O-GlcNAcylation and O-GlcNAc Cycling Regulate Gene Transcription: Emerging Roles in Cancer. Cancers *13*, 1666. https://doi.org/10.3390/cancers13071666.
40. Lu, Y., Labak, C.M., Jain, N., Purvis, I.J., Guda, M.R., Bach, S.E., Tsung, A.J., Asuthkar, S., and Velpula, K.K. (2017). OTX2 expression contributes to proliferation and progression in Myc-amplified medulloblastoma. Am. J. Cancer Res. *7*, 647–656.
41. Itkonen, H.M., Loda, M., and Mills, I.G. (2021). O-GlcNAc Transferase - An Auxiliary Factor or a Full-blown Oncogene? Mol. Cancer Res. *19*, 555–564. https://doi.org/10.1158/1541-7786.MCR-20-0926.
42. Shafi, R., Iyer, S.P., Ellies, L.G., O'Donnell, N., Marek, K.W., Chui, D., Hart, G.W., and Marth, J.D. (2000). The O-GlcNAc transferase gene resides on the X chromosome and is essential for embryonic stem cell viability and mouse ontogeny. Proc. Natl. Acad. Sci. USA *97*, 5735–5739. https://doi.org/10.1073/pnas.100471497.
43. Olivier-Van Stichelen, S., Wang, P., Comly, M., Love, D.C., and Hanover, J.A. (2017). Nutrient-driven *O*-linked *N*-acetylglucosamine (*O*-GlcNAc) cycling impacts neurodevelopmental timing and metabolism. J. Biol. Chem. *292*, 6076–6085. https://doi.org/10.1074/jbc.M116.774042.
44. Heimbucher, T., Murko, C., Bajoghli, B., Aghaallaei, N., Huber, A., Stebegg, R., Eberhard, D., Fink, M., Simeone, A., and Czerny, T. (2007). Gbx2 and Otx2 interact with the WD40 domain of Groucho/Tle corepressors. Mol. Cell Biol. *27*, 340–351. https://doi.org/10.1128/MCB.00811-06.
45. Yang, S.H., Kalkan, T., Morissroe, C., Marks, H., Stunnenberg, H., Smith, A., and Sharrocks, A.D. (2014). Otx2 and Oct4 drive early enhancer activation during embryonic stem cell transition from naive pluripotency. Cell Rep. *7*, 1968–1981. https://doi.org/10.1016/j.celrep.2014.05.037.
46. Vriend, J., and Rastegar, M. (2020). Ubiquitin ligases and medulloblastoma: genetic markers of the four consensus subgroups identified through transcriptome datasets. Biochim. Biophys. Acta, Mol. Basis Dis. *1866*, 165839. https://doi.org/10.1016/j.bbadis.2020.165839.
47. Fant, B., Samuel, A., Audebert, S., Couzon, A., El Nagar, S., Billon, N., and Lamonerie, T. (2015). Comprehensive interactome of *Otx2* in the adult mouse neural retina: Interactome of Otx2 in the mouse neural retina. genesis *53*, 685–694. https://doi.org/10.1002/dvg.22903.
48. Wang, D.w., Peng, Z.j., Ren, G.f., and Wang, G.x. (2015). The different roles of selective autophagic protein degradation in mammalian cells. Oncotarget *6*, 37098–37116. https://doi.org/10.18632/oncotarget.5776.
49. Stoebel, D.M., Dean, A.M., and Dykhuizen, D.E. (2008). The cost of expression of Escherichia coli lac operon proteins is in the process, not in the products. Genetics *178*, 1653–1660. https://doi.org/10.1534/genetics.107.085399.
50. Choudhury, S., Kolukula, V.K., Preet, A., Albanese, C., and Avantaggiati, M.L. (2013). Dissecting the pathways that destabilize mutant p53: The proteasome or autophagy? Cell Cycle *12*, 1022–1029. https://doi.org/10.4161/cc.24128.
51. Petherick, K.J., Williams, A.C., Lane, J.D., Ordóñez-Morán, P., Huelsken, J., Collard, T.J., Smartt, H.J.M., Batson, J., Malik, K., Paraskeva, C., and Greenhough, A. (2013). Autolysosomal β-catenin degradation regulates Wnt-autophagy-p62 crosstalk. EMBO J. *32*, 1903–1916. https://doi.org/10.1038/emboj.2013.123.
52. Chang, C.-P., Su, Y.-C., Hu, C.-W., and Lei, H.-Y. (2013). TLR2-dependent selective autophagy regulates NF-κB lysosomal degradation in hepatoma-derived M2 macrophage differentiation. Cell Death Differ. *20*, 515–523. https://doi.org/10.1038/cdd.2012.146.
53. Liu, X.-D., Zhu, H., DePavia, A., and Jonasch, E. (2015). Dysregulation of HIF2α and autophagy in renal cell carcinoma. Mol. Cell. Oncol. *2*, e965643. https://doi.org/10.4161/23723548.2014.965643.
54. Lamark, T., and Johansen, T. (2012). Aggrephagy: Selective Disposal of Protein Aggregates by Macroautophagy. Int. J. Cell Biol. *2012*, 736905–736921. https://doi.org/10.1155/2012/736905.
55. Zhang, F., Su, K., Yang, X., Bowe, D.B., Paterson, A.J., and Kudlow, J.E. (2003). O-GlcNAc modification is an endogenous inhibitor of the proteasome. Cell *115*, 715–725.
56. Yang, W.H., Kim, J.E., Nam, H.W., Ju, J.W., Kim, H.S., Kim, Y.S., and Cho, J.W. (2006). Modification of p53 with O-linked N-acetylglucosamine regulates p53 activity and stability. Nat. Cell Biol. *8*, 1074–1083. https://doi.org/10.1038/ncb1470.
57. Han, I., and Kudlow, J.E. (1997). Reduced O glycosylation of Sp1 is associated with increased proteasome susceptibility. Mol. Cell Biol. *17*, 2550–2558. https://doi.org/10.1128/MCB.17.5.2550.
58. Olivier-Van Stichelen, S., Dehennaut, V., Buzy, A., Zachayus, J.-L., Guinez, C., Mir, A.-M., El Yazidi-Belkoura, I., Copin, M.-C., Boureme, D., Loyaux, D., et al. (2014). O-GlcNAcylation stabilizes β-catenin through direct competition with phosphorylation at threonine 41. FASEB J. Off. Publ. Fed. Am. Soc. Exp. Biol. *28*, 3325–3338. https://doi.org/10.1096/fj.13-243535.
59. Trinidad, A.G., Muller, P.A.J., Cuellar, J., Klejnot, M., Nobis, M., Valpuesta, J.M., and Vousden, K.H. (2013). Interaction of p53 with the CCT Complex Promotes Protein Folding and Wild-Type p53 Activity. Mol. Cell *50*, 805–817. https://doi.org/10.1016/j.molcel.2013.05.002.
60. Pavel, M., Imarisio, S., Menzies, F.M., Jimenez-Sanchez, M., Siddiqi, F.H., Wu, X., Renna, M., O'Kane, C.J., Crowther, D.C., and Rubinsztein, D.C. (2016). CCT complex restricts neuropathogenic protein aggregation via autophagy. Nat. Commun. *7*, 13821. https://doi.org/10.1038/ncomms13821.
61. Montalta-He, H., Leemans, R., Loop, T., Strahm, M., Certa, U., Primig, M., Acampora,

D., Simeone, A., and Reichert, H. (2002). Evolutionary conservation of otd/Otx2 transcription factor action: a genome-wide microarray analysis in Drosophila. Genome Biol. *3*. RESEARCH0015. https://doi.org/10.1186/gb-2002-3-4-research0015.

62. Gregory, L.C., Gergics, P., Nakaguma, M., Bando, H., Patti, G., McCabe, M.J., Fang, Q., Ma, Q., Ozel, A.B., Li, J.Z., et al. (2021). The phenotypic spectrum associated with OTX2 mutations in humans. Eur. J. Endocrinol. *185*, 121–135. https://doi.org/10.1530/EJE-20-1453.

63. Bernard, C., Kim, H.-T., Torero Ibad, R., Lee, E.J., Simonutti, M., Picaud, S., Acampora, D., Simeone, A., Di Nardo, A.A., Prochiantz, A., et al. (2014). Graded Otx2 activities demonstrate dose-sensitive eye and retina phenotypes. Hum. Mol. Genet. *23*, 1742–1753. https://doi.org/10.1093/hmg/ddt562.

64. Ragge, N.K., Brown, A.G., Poloschek, C.M., Lorenz, B., Henderson, R.A., Clarke, M.P., Russell-Eggitt, I., Fielder, A., Gerrelli, D., Martinez-Barbera, J.P., et al. (2005). Heterozygous Mutations of OTX2 Cause Severe Ocular Malformations. Am. J. Hum. Genet. *76*, 1008–1022. https://doi.org/10.1086/430721.

65. Livak, K.J., and Schmittgen, T.D. (2001). Analysis of Relative Gene Expression Data Using Real-Time Quantitative PCR and the $2^{-\Delta\Delta CT}$ Method. Methods *25*, 402–408. https://doi.org/10.1006/meth.2001.1262.

66. Kim, E., Kang, J.G., Kang, M.J., Park, J.H., Kim, Y.J., Kweon, T.H., Lee, H.-W., Jho, E.H., Lee, Y.H., Kim, S.-I., et al. (2020). *O*-GlcNAcylation on LATS2 disrupts the Hippo pathway by inhibiting its activity. Proc. Natl. Acad. Sci. USA *117*, 14259–14269. https://doi.org/10.1073/pnas.1913469117.

67. Brademan, D.R., Riley, N.M., Kwiecien, N.W., and Coon, J.J. (2019). Interactive Peptide Spectral Annotator: A Versatile Web-based Tool for Proteomic Applications. Mol. Cell. Proteomics *18*, S193–S201. https://doi.org/10.1074/mcp.TIR118.001209.

68. Jumper, J., Evans, R., Pritzel, A., Green, T., Figurnov, M., Ronneberger, O., Tunyasuvunakool, K., Bates, R., Žídek, A., Potapenko, A., et al. (2021). Highly accurate protein structure prediction with AlphaFold. Nature *596*, 583–589. https://doi.org/10.1038/s41586-021-03819-2.

69. Conchillo-Solé, O., de Groot, N.S., Avilés, F.X., Vendrell, J., Daura, X., and Ventura, S. (2007). AGGRESCAN: a server for the prediction and evaluation of "hot spots" of aggregation in polypeptides. BMC Bioinf. *8*, 65. https://doi.org/10.1186/1471-2105-8-65.

STAR★METHODS

KEY RESOURCES TABLE

REAGENT or RESOURCE	SOURCE	IDENTIFIER
Antibodies		
Rabbit polyclonal anti-OTX2	Proteintech	Cat# 13497-1-AP; RRID:AB_2157176
Mouse monoclonal anti-*O*-Linked N-Acetylglucosamine antibody (RL2)	Abcam	Cat# ab2739; RRID:AB_303264
Rabbit polyclonal anti-Actin	Millipore Sigma	Cat# A2066; RRID:AB_476693
Mouse monoclonal anti-β-Actin	Millipore Sigma	Cat# A5441; RRID:AB_476744
Mouse monoclonal anti-Ubiquitin (eBioP4D1 (P4D1))	Thermo Fisher Scientific	Cat# 14-6078-82; RRID:AB_837154
Rabbit polyclonal anti-LC3B	Proteintech	Cat# 18725-1-AP; RRID:AB_2137745
Rabbit polyclonal anti-*c*-Myc	Millipore Sigma	Cat# C3956; RRID:AB_439680
Mouse monoclonal anti-DYKDDDDK (FLAG) Tag (FG4R)	Thermo Fisher Scientific	Cat# MA1-91878; RRID:AB_1957945
Mouse monoclonal anti-alpha-Tubulin (961258)	Novus Biologicals	Cat# MAB93441; RRID:AB_2938603
Rabbit polyclonal anti-Lamin A/C	Novus Biologicals	Cat# NB100-56649; RRID:AB_838524
Mouse monoclonal anti-GAPDH	Abcam	Cat# ab9484; RRID:AB_307274
Rabbit polyclonal anti-CCT5	Bethyl Laboratories	Cat# A303-481A; RRID:AB_10952578
Rabbit polyclonal anti-SQSTM1/p62	Abcam	Cat# ab91526; RRID:AB_2050336
Bacterial and virus strains		
One Shot™ BL21 Star™ (DE3) Chemically Competent *E. coli* cells	Invitrogen	Cat# C601003
Chemicals, peptides, and recombinant proteins		
Thiamet G	Millipore Sigma	Cat# SML0244
Chloroquine diphosphate salt	Chem Impex	Cat# 22113
MG-132	Millipore Sigma	Cat# 474790
Bortezomib	Millipore Sigma	Cat# 504314
Cycloheximide	Millipore Sigma	Cat# 01810
PUGNAc	Millipore Sigma	Cat# A7229
Doxycycline	TCI Chemicals	Cat# D4116
OSMI4	MedChemExpress	Cat# HY-114361
DRB	Millipore Sigma	Cat# D1916
Rapamycin	Cell Signaling	Cat# 9904
DSP	Pierce	Cat# A35393
Phos binding reagent acrylamide	ApexBio	Cat# F4002
Lambda Protein Phosphatase	New England BioLabs	Cat# P0753S
Critical commercial assays		
In-Fusion Snap assembly	Takara	Cat# 638947
QuikChange II Site-Directed Mutagenesis Kit	Agilent Technologies	Cat# 200523
Pierce Glycoprotein Isolation Kit, WGA	Thermo Fisher Scientific	Cat# 89805
Phospha-Light SEAP Reporter Gene Assay System	Invitrogen	Cat# T1017
Renilla Luciferase Assay System	Promega	Cat# E2810
MTT Cell Proliferation/Viability Assay	R&D Systems	Cat# 4890-050-K
Strep-Tactin® HRP conjugate	IBA Lifesciences	Cat# 2-1502-001

(*Continued on next page*)

Continued

REAGENT or RESOURCE	SOURCE	IDENTIFIER
Pierce™ Anti-DYKDDDDK Magnetic Agarose (Anti-Flag)	Thermo Fisher Scientific	Cat# A36797
Strep-Tactin® Sepharose® resin	IBA Lifesciences	Cat# 2-1201-002
Deposited data		
Mass spectrometry proteomics	ProteomeXchange	PXD040353
Experimental models: Cell lines		
A6#20 D425 human medulloblastoma	Dr. Veersteg and Dr. Kool (University of Amsterdam)	
HeLa	Dr. B Smith (MCW)	
MCF7	Dr J.A. Hanover (NIH)	
Oligonucleotides		
Primer: Actb-F ACCATGGATGATGATATCGC		
Primer: Actb-R TCATTGTAGAAGGTGTGGTG		
Primer: Otx2-F GAAAATCAACTTGCCAGAATCCA		
Primer: Otx2-R GCGGCACTTAGCTCTTCGAT		
Recombinant DNA		
pETDuet-hOGT-hOTX2-FLAG	Sigma-Aldrich, 71146	
pDEST47-Empty	This paper	
pDEST47-OTX2-FL	This paper	
pDEST47-RD	This paper	
pDEST47-ΔRD	This paper	
pDEST47-HD	This paper	
pDEST47-OT	This paper	
pDEST47-TFT	This paper	
OTX2-Myc-DDK	Origen(#rc207479)	
OTX2	Origen(#rc207479)	
pCAG-OTX2-OSF	This paper	
pCAG-OTX2(S135A)-OSF	This paper	
pCAG-OTX2(S136A)-OSF	This paper	
pCAG-OTX2(T137A)-OSF	This paper	
pCAG-OTX2(S138A)-OSF	This paper	
pCAG-OTX2(S135A/S136A/T137A)-OSF	This paper	
pCAG-OTX2(S135A/S136A/T137A/S138A)-OSF	This paper	
OTX2-GFP	T. Lamonerie, PHD (IBV, France)	
OTX2(S136A)-GFP	T. Lamonerie, PHD (IBV, France)	
OTX2(T137A)-GFP	T. Lamonerie, PHD (IBV, France)	
OTX2(S135A/S136A/T137A)-GFP	T. Lamonerie, PHD (IBV, France)	
IRBP-SEAP	T. Lamonerie, PHD (IBV, France)	
pRL	Promega, E2231	
Software and algorithms		
AlphaFold		
PyMOL		
Cytoscape		
STRING		
AGGRESCAN		

(*Continued on next page*)

Continued

REAGENT or RESOURCE	SOURCE	IDENTIFIER
Biorender		
GraphPad Prism		
Spectrum annotator web tool		
Proteome Discoverer 2.4		

RESOURCE AVAILABILITY

Lead contact

Further information and requests for resources and reagents should be directed to and will be fulfilled by the lead contact, Stephanie Olivier-Van Stichelen (solivier@mcw.edu).

Materials availability

Plasmids are available upon request.

Data and code availability

The mass spectrometry proteomics data have been deposited to the ProteomeXchange Consortium via the PRIDE partner repository with the dataset identifier PXD040353 and are publicly available as of the date of publication. This paper does not report original code. Any additional information required to reanalyze the data reported in this paper is available from the lead contact upon request.

EXPERIMENTAL MODEL

Cell culture

All cell lines were maintained at 37°C in a 5% (v/v) CO2-enriched humidified atmosphere, and tested regularly for mycoplasma contamination. Authenticated A6#20 D425 Human Medulloblastoma Cells were gifted from Dr. Versteeg and Dr. Kool.[17] They possess a doxycycline-inducible shRNA against OTX2. A6#20 cells were cultured in Minimum Essential Medium (MEM) supplemented with 10% newborn calf serum, 1% penicillin/streptomycin, 200 nM L-glutamine, as well as the antibiotics Blasticidin S hydrochloride, and Zeocin (Alfa Aesar, 4 μg/mL and 25 μg/mL routine concentration, respectively), for maintenance of the doxycycline-inducible *OTX2* shRNA.

HeLa and MCF7 cells were maintained in DMEM supplemented with 10% fetal bovine serum and 1% Penicillin/Streptomycin.

Recombinant protein expression in E. coli

One Shot BL21 Star (DE3) Chemically Competent *E. coli* (Invitrogen) cells were transformed with 5–10 ng of plasmid DNA (pETDuet-hOGT-hOTX2-FLAG) according to the manufacturer's instructions. For protein expression, transformants were inoculated into LB media containing ampicillin (100 μg/mL) and grown overnight at 37°C, shaking at 225 rpm. The culture was then diluted to reach optical density at 600 nm (OD600) of 0.1 and incubated with shaking at 37°C until OD600 reached 0.6. To induce protein expression, 0.5 mM isopropyl β-D-1-thiogalactopyranoside (IPTG) was added to the culture media for 2 h shaking and incubated at 30°C.

METHOD DETAILS

Drugs and inhibitors

Drugs were resuspended in sterile distilled water unless otherwise stated and used at the following concentration: Thiamet G (Millipore Sigma) at 100 nM, Chloroquine diphosphate salt (Chem-Impex) at 50 μM, MG-132 (Millipore Sigma) at 2 μM (DMSO), Bortezomib (BTZ) (Millipore Sigma) at 330 nM, Cycloheximide (Millipore Sigma) at 50 μg/mL, doxycycline (DOX) (TCI Chemicals) at 100 ng/mL, OSMI4 (MedChemExpress) at 5 μM (DMSO); 5,6-dichlorobenzimidazole 1-beta-D-ribofuranoside (DRB) (Millipore Sigma) at 50 μM (DMSO), and Rapamycin (Cell Signaling) at 1μM.

Plasmids and transient transfections

All constructs were cloned into the pE3n cloning vector before expression plasmids. Gateway technology (LifeTechnologies) was used to insert the constructs into the pDEST47 backbone for mammalian expression. Alternatively, InFusion cloning (Takara Bio) was used to create protein domain deletions and insert constructs into every other plasmid backbone. Point mutations were inserted using the QuickChange II kit (Agilent Technologies). Sequences were verified by Sanger sequencing. Myc-DDK-tagged-OTX2 (Origene) was used as a template for OTX2 cloning. Transfection of plasmids was done using Lipofectamine 2000 or Lipofectamine 3000 reagents according to manufacturer instructions (ThermoFisher Scientific). Cells were transfected with corresponding plasmids 24 h before treatments with inhibitors.

RNA extraction, cDNA synthesis, and quantitative PCR

Total RNAs were purified with the RNeasy mini kit (Qiagen) according to the manufacturer's instructions. On-column DNAse digestion (Qiagen) was additionally performed to remove genomic DNA. RNA concentration was measured using a nanodrop dosage spectrophotometer, and quality was checked by running RNA on an agarose gel and analyzing the integrity of ribosomal RNA (28 S and 18 S). RNA extract (500 μg) was converted to cDNA with qScript cDNA Supermix (Quanta Bioscience) according to the manufacturer's instructions. Total cDNA was then quantified using a nanodrop spectrophotometer. Gene Expression was measured using fast SYBR Green Master Mix (Applied Biosystems), 1 μg of cDNA, and the specific primer pair. Quantitative PCR was run on an AB 7900HT fast real-time PCR system (Applied Biosystems). Each experiment was performed in triplicate and analyzed by calculating the $2^{-\Delta\Delta CT}$ (Livak and Schmittgen[65]) relative to actin expression.

Primers

For endogenous control, Actb-F (ACCATGGATGATGATATCGC) and Actb-R (TCATTGTAGAAGGTGTGGTG). For *Otx2* expression, Otx2-F (GAAAATCAACTTGCCAGAATCCA) and Otx2-R (GCGGCACTTAGCTCTTCGAT).

Cell lysis

For mammalian cells, samples were lysed for 5–10 min in radioimmunoprecipitation assay lysis buffer (RIPA) (10-mM Tris-HCl, 150-mM NaCl, 1% Triton X-100 [v/v], 0.5% NaDOC [w/v], 0.1% sodium dodecyl sulfate [w/v], 10 μM PUGNAc, and protease inhibitors; pH 7.5), vortexed and centrifuged 20 min at 18000 × g at 4°C.

To extract protein from the bacterial preparation, the culture was centrifuged at 3220 x g for 10 min at 4°C. The pellet was either stored at −80°C if not used immediately or resuspended in RIPA buffer for protein purification (see Cell lysis for buffer composition). DNA was sheared by sonicating lysates for 5 cycles of 5-s pulses on ice, and lysates were cleared by centrifugation for 20 min at 18000 × g at 4°C.

Nuclear and cytosol fractionation

Protocol adapted from.[66] Cells were incubated in ice-cold hypotonic buffer (5 mM Tris pH 7.5, 100 μM dithiothreitol (DTT), 50 μM ethylenediaminetetraacetic acid (EDTA), and 0.5% Nonidet P-40) for 15 min and centrifuged at 3400 × g for 3 min at 4°C. The supernatant was retained as the cytosolic fraction, and the pellet was washed with PBS and centrifuged again at 3400 × g for 3 min at 4°C. To obtain the nuclear fraction, the pellet was incubated in RIPA buffer on ice for 10 to 15 min and centrifuged at 18000 × g for 10 min at 4°C. The supernatant of the lysed pellet was collected as the nuclear fraction.

Immunoprecipitation (IP) and pulldowns

O-GlcNAcylated proteins were pulled down using the Pierce Glycoprotein Isolation Kit, WGA (ThermoFisher Scientific), according to the manufacturer's protocol. Flowthrough lysate was saved as the unbound sample, while the beads were saved as the WGA sample.

Pierce Anti-DYKDDDDK Magnetic Agarose (Anti-Flag) (Thermo Scientific) was used according to manufacturer instructions. Beads were washed 4 times with RIPA and 3 times with PBS. After washes with lysis buffer and PBS, beads were either boiled in 1X Laemmli buffer (50 mM Tris-HCl pH6.8, 2% SDS, 10% glycerol, 5% 2-mercapto-ethanol (BME), and 0.005% Bromophenol Blue) for SDS-PAGE or processed for mass spectrometry analysis.

Strep-Tactin Sepharose resin (IBA Lifesciences) was used to purify OTX2-OSF (and site mutants) produced in HeLa cells. Used 25 μL of slurry per lysate sample (from a 6-well plate). Equilibrated beads in RIPA buffer were incubated with protein lysates at 4°C overnight with rotation in a Biomixer 3D Nutating Shaker (Benchmark Scientific). Beads were processed for further analysis after washes with lysis buffer and PBS.

SDS-PAGE and western blotting

Laemmli Buffer was added to each protein lysate and boiled at 95°C for 5 min before separation by SDS-PAGE. Samples were resolved on 12% or 4–20% Tris-glycine gels and transferred onto nitrocellulose. Membranes were blocked for 45 min with 5% [w/v] nonfat milk in Tris-buffered saline-Tween 20 (0.1% [v/v]) buffer (TBS-T). Primary antibodies were incubated overnight at 4°C with gentle agitation in milk/TBST. Following primary incubation, blots were washed 3 times with 10 mL of TBS-T for 10 min and incubated with anti-mouse and anti-rabbit fluorescent-conjugated secondary antibodies (LICOR) in a 1:10000 dilution for 1 h at room temperature. Three additional TBS-T washes with 10 mL in 10 min were performed. One final PBS wash for 5 min was performed, and the blot was imaged on the Odyssey Fc imager (LI-COR).

PhosTag gels

Phos binding reagent acrylamide (ApexBio), labeled as PhosTag in the text, was used when mentioned as instructed by manufacturers for phosphorylation assessment. PhosTag SDS-PAGE gels were prepared with 10% acrylamide, 0.1 mM $MnCl_2$, 0.1% SDS, and 50 mM PB-A (phos-bind reagent). After electrophoresis, gels were soaked in 10 mM EDTA solution 3 times for 10 min each wash before soaking in transfer buffer for Western blot as outlined above. A phosphatase treatment was performed in a 50ul reaction using 400 units of Lambda Protein Phosphatase (New England BioLabs), incubated with protein lysate at 30C for 30 min, according to the manufacturer's instructions, prior to loading in a PhosTag gel.

SEAP gene reporter assay

HeLa cells were co-transfected with 3 plasmids— 1) One containing the region −66 to +68 of the *IRBP* promoter cloned into the pSEAP2-basic vector to assay OTX2 transcriptional activity,[38] 2) One plasmid coding for either WT OTX2-OSF, 3A OTX2-OSF, or empty vector EV-OSF, 3) One plasmid containing the pRL *Renilla* luciferase gene under the control of a CMV promoter to normalize for transfection efficiency (Promega). Sixteen hours after transfection, culture media was changed, and initial treatment with inhibitors was started (TG, OSMI4, DRB, or DMSO). Eight hours post-treatment, culture media was stored for further analysis, and cells received fresh media with inhibitors. Seventeen hours after the second treatment, a culture media sample was taken, and cells were incubated for 4 more hours. Finally, the rest of the culture media was stored, and the cells were harvested in 250ul of *Renilla* Luciferase Assay Lysis Buffer. Secreted alkaline phosphatase (SEAP) activity in the culture media samples was measured with the Phospha-Light SEAP Reporter Gene Assay System (Invitrogen) according to the manufacturer's protocol. *Renilla* luciferase levels in the cell lysates were measured using the *Renilla* Luciferase Assay System (Promega). SEAP activity values were normalized to the corresponding cell lysate's *Renilla* levels.

Protein aggregation assay

The membrane-permeable thiol-cleavable Dithiobis (succinimidyl Propionate) (DSP) compound was used to preserve intracellular oligomers. DSP (Pierce) was dissolved in DMSO for the stock solution and further diluted in warm PBS to a working concentration (crosslinker solution, 1 mM unless stated otherwise). A6#20 cells were treated overnight with degradation inhibitors, and HeLa cells were transfected with OTX2 WT and 3A plasmids 24 h before DSP treatment. Cells were then washed twice with warm PBS before incubation with the crosslinker solution for 30 min at room temperature. The crosslinking reaction was stopped by adding 1M Tris HCl pH 7.4 to the cells to a final concentration of 10 mM and incubating for 15 min at room temperature. Cells were washed twice with cold PBS and lysed in 200ul RIPA buffer. Lysates were vortexed and cleared by centrifugation at 18000xg for 30 min at 4°C. The supernatant was saved as soluble proteins, while the pellet was lysed in 100ul RIPA buffer and sonicated (10 × 1 s pulses) to break apart the pellet and decrease viscosity. Both the soluble protein lysate and the pellet lysate were prepared in Laemmli buffer, with or without BME, and heated at 65C for 5 min. Samples in Laemmli were not further centrifuged before loading on 4–20% gels. When transferring proteins to the nitrocellulose membrane, we ensured the bottom of the loading wells were present for transfer.

Antibodies

Antibodies for Western blotting were used as follows, diluted 1:1000 unless noted otherwise: Anti-OTX2 (Proteintech); Anti-*O*-GlcNAc (RL2, Abcam); Anti-actin produced in rabbit (Sigma Aldrich), 1:2000; Anti-β-actin produced in mouse (Sigma Aldrich), 1:2000; Anti-ubiquitin (P4D1, ThermoFisher Scientific), 1:250; Anti-LC3B (Proteintech); Anti-*c*-Myc (Millipore Sigma), 1:2000; Anti-DYKDDDDK tag (FLAG, FG4R, Invitrogen); Anti-α-tubulin (Novus Biologicals); Anti-lamin A/C (Novus Biologicals); Strep-Tactin HRP conjugate (IBA Lifesciences) used as instructed in manufacturer's protocol; GAPDH (Abcam); CCT5 (Bethyl Laboratories); SQSTM1/p62 (Abcam).

Confocal microscopy

Cells transfected with GFP-tagged protein were washed with PBS and fixed in freshly made 4% formaldehyde/PBS for 15 min at room temperature. After three PBS washes (5 min each), mounted in DAPI/fluoromount G (Electron Microscopy Sciences) and observed under a confocal microscope (Cytation10).

For immunofluorescent staining, cells transfected with OTX2-Myc-DDK were cultured in chamber slides. First, cells were washed with PBS and fixed as outlined above. Then, cells were permeabilized for 10 min with 0.1% Triton X-100 in PBS (PBS-T) and subsequently blocked with 1% BSA in PBS-T solution for 30 min. Slides were incubated with primary antibodies in 1% BSA in PBS-T in a humidified chamber overnight at 4°C, then the cells were washed three times in PBS-T for 5 min each, incubated with secondary antibodies in 1% BSA for 1 h at room temperature protected from light, and finally washed three times with PBST for 5 min each in the dark. The nuclei were then stained with DAPI for 3 min, rinsed with PBS-T, and coverslips were mounted using a water-soluble mounting media.

MTT cell proliferation assay

Proliferation assays were performed using the Cell Proliferation Kit I (MTT) (R&D systems) according to the manufacturer's protocol. Briefly, HeLa cells were seeded at 2.5×10^4 cells/well in a 96-well plate and transfected with either WT, 3A, or empty vector EV-OSF. Sixteen hours after transfection, cells were treated with inhibitors for 24 h. Each condition was performed in 6 replicates, and measurements were averaged. A total of 10 μL of the MTT reagent was added to each well for 3 h. Then, 100 μL of the solubilization solution was added overnight before measuring absorbance at 570 nm.

Mass spectrometry

The pulldown beads were resuspended in 100 μL of 40% Invitrosol and 100 mM ammonium bicarbonate. Cysteines were reduced in 5 mM TCEP for 30 min at 37°C and alkylated with 10 mM iodoacetamide for 30 min at 37°C. The bead-bound proteins were then digested overnight with 5 μg of trypsin at 37°C followed by cleanup using the SP2 method. Thermo Scientific Pierce Peptide Retention Time Calibration Mixture added at 4 nM concentration during dilution of the samples to 25 ng/μL. For *O*-GlcNAc site mapping of recombinant OTX2, each sample was analyzed on a Thermo Scientific Orbitrap Fusion Lumos MS via two technical replicate injections in each of two methods, one using HCD and

product ion triggered EThcD, the other HCD and EThcD for all MS2 spectra. To obtain the OTX2 interactome by mass spectrometry, each sample was analyzed on a Orbitrap Fusion Lumos MS via 3 technical replicate injections using a data-dependent acquisition (DDA) HCD MS2 instrument method. The technical replicates were blocked, and each block was randomized. Pooled QCs, which is a mixture of all the samples being analyzed, was analyzed at the start, end, and in between each sample. Protein identifications were filtered to include only those proteins identified by two or more unique peptides identified. All MS data were analyzed using Proteome Discoverer 2.4 (Thermo) platform. See Table S4 for further details regarding the methods used and data analysis performed. Graphs with annotated peptides were generated using the spectrum annotator web tool.[67]

In silico analysis

The predicted full-length OTX2 protein structure was obtained from the AlphaFold protein structure database[68] and annotated using PyMOL. Aggregation analyses were performed on the AGGRESCAN software.[69] Interaction networks were generated with Cytoscape using the STRING database.[35] Network color-codes were performed by grouping manually according to similarities in molecular function, biological process, and subcellular localization.

QUANTIFICATION AND STATISTICAL ANALYSIS

Blot quantification was performed by Optical Density (OD) measurement. Each qPCR experiment was performed in triplicate and analyzed by calculating the $2^{-\Delta\Delta CT}$[65] relative to actin expression. Statistical analyses were performed on Prism 9 (GraphPad). Error bars represent the mean $\pm$ standard error of the mean (SEM). A classic Student's *t* test (unpaired, parametric) or one-way/two-way ANOVA was performed to assess significance, as specified in figure legends. Statistical significance was always represented as follows: ns $\geq$ 0.05, *p < 0.05, **p < 0.01, ***p < 0.001, ****p < 0.0001.